Article

Radon Variability as a Result of Interaction with the Environment

Sergey Pulinets [1,*], Irina Mironova [2,*], Petr Miklyaev [3], Tatiana Petrova [4], Alexander Shitov [5] and Arseniy Karagodin [2]

1   Space Research Institute RAS, Profsoyuznaya Str. 84/32, 117997 Moscow, Russia
2   Saint-Peresburg State University, Universitetskaya Emb.7-9, 199034 St. Petersburg, Russia; karars94@mail.ru
3   Sergeev Institute of Environmental Geoscience RAS (IEG RAS), Ulansky per. 13, Build. 2, 101000 Moscow, Russia; mik@geoenv.ru
4   Faculty of Chemistry, Lomonosov Moscow State University, Leninskie Gory 1, Build. 3, GSP-1, 119991 Moscow, Russia; tbp111@inbox.ru
5   Gorno-Altaisk State University, Lenkin St. 1, 649000 Gorno-Altaisk, Russia; sav103@yandex.ru
*   Correspondence: pulse@cosmos.ru (S.P.); i.a.mironova@spbu.ru (I.M.)

Abstract: Recent years have seen increased attention given to radon from two scientific directions. After neglecting radon as an earthquake precursor in the 1990s, it has become the subject of discussions in earthquake-forecast papers due to growing networks of radon monitoring in different countries, particularly the technologies of real-time radon measurements where gamma spectrometers are of great interest as sources of ^{222}Rn identification. The second fast-developing direction involves radon in Lithosphere–Atmosphere–Ionosphere Coupling (LAIC) models as a source of boundary layer ionization. Here we address the second topic, which is not connected with the earthquake forecast problems, namely, the role of air ionization by radon as a source of the Global Electric Circuit (GEC) modification. In this publication, we try to unite all of these problems to present a more complex view of radon as an important element in our environment. Special attention is paid to the dependence of radon variability on environmental conditions.

1. Introduction

Radon, an odorless noble gas, is radioactive and belongs to the VIII group of Mendeleev's periodic table. Its atomic number is 86, and it has three natural isotopes: ^{219}Rn, ^{220}Rn, and ^{222}Rn. ^{219}Rn is a member of the actinon–uranium decay chain, so it is usually named 'actinon' with the symbol An. Its semi-decay period is 3.92 s. ^{220}Rn is a member of the Thorium decay chain and usually named 'thoron' (Tn); its semi-decay period is 54.5 s. The third, and actually most important, isotope ^{222}Rn from the uranium–radium decay chain is radon itself, and the symbol Rn is attributed just to this isotope. Its semi-decay period is 3.823 days. One can see the decay trees of main radon isotopes in Figure 1, and major parameters of main radon isotopes and their progenies are given in Table 1. The discovery of radon as an emanation of radium is attributed to German physicist Friedrich Ernst Dorn [1] in 1900. Thoron was described by Rutherford and Owens one year earlier [2], and the discovery of actinon in 1903 is attributed to Andre Louis Debierne [3]. Some physicists including Rutherford proposed to name it "emanation" but finally, because it is a radium progeny, it was named radon. Radon was the first chemical element showing the possibility to have isotopes. The mass concentration of radon in the Earth's atmosphere is near 6×10^{-17}%.
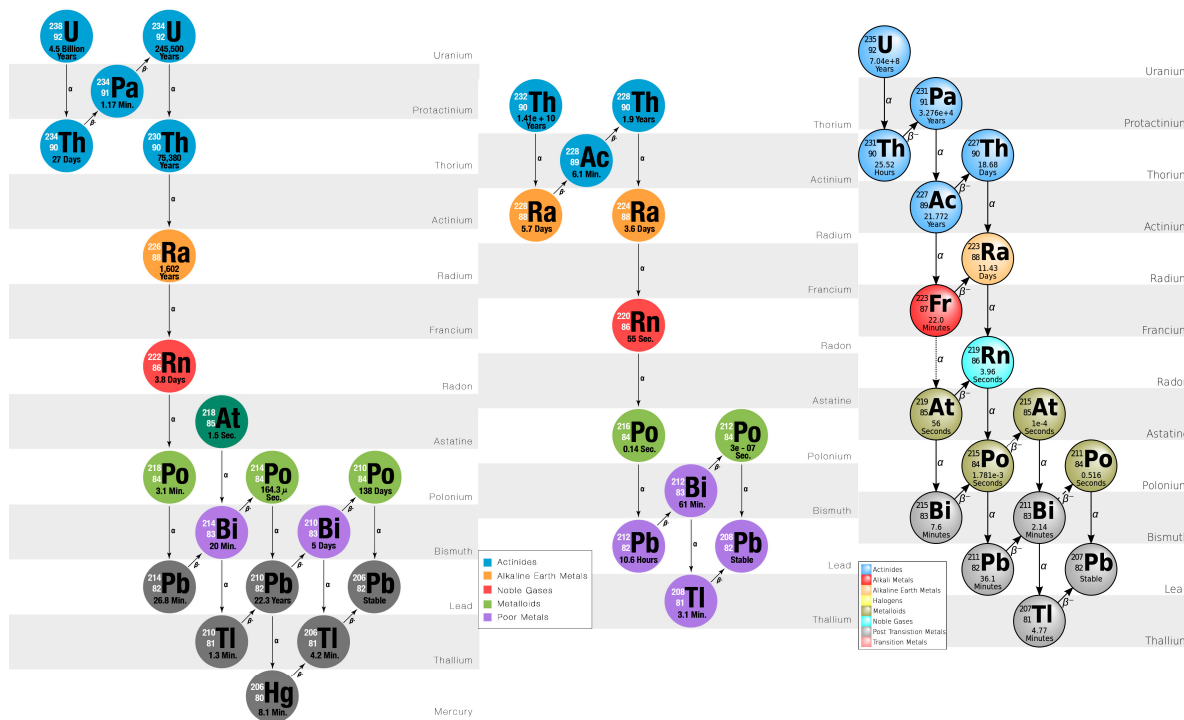
Figure 1. Decay trees of the main radon isotopes finished by stable elements. (**Left**) ^{222}Rn (red circle) decay chain; (**middle**) ^{220}Rn (red circle) named thoron decay chain; (**right**) ^{219}Rn (turquoise circle) named actinon decay chain. All images copyright © 2024–2024 the International Association of Certified Home Inspectors, Inc. (InterNACHI). https://www.nachi.org/gallery/ (accessed on 21 January 2024).

Table 1. Uranium decay products.

Nuclide	Historic Name (Short)	Historic Name (Long)	Decay Mode	Half Life	MeV	Product of Decay
^{222}Rn	Rn	Radon	α	3.8235 d	5.590	^{218}Po
^{220}Rn	Tn	Thoron	α	55.6 s	6.4047	^{224}Ra
^{219}Rn	An	Actinon	α	3.96 s	6.946	^{223}Ra
^{218}Po	RaA	Radium A Polonium	α β$^-$	3.10 min	6.115 0.265	^{214}Pb ^{218}At
^{218}At		Astatine	α β$^-$	1.5 s	6.874 2.883	^{214}Bi ^{218}Rn
^{218}Rn			α	35 ms	7.263	^{214}Po
^{214}Pb	RaB	Radium B	β$^-$	26.8 min	1.024	^{214}Bi
^{214}Bi	RaC	Radium C	β α$^-$	19.9 min	3.272 5.617	^{214}Po ^{210}Tl
^{214}Po	RaC′	Radium C′	α	0.1643 ms	7.883	^{210}Pb

During its decay, radon emits α-particles which are actually the helium nucleus. It should be noted that nearly 99% of the helium produced is the result of the alpha decay of underground deposits of minerals containing uranium or thorium. Radon radioactivity could be used as a tracer. In the case of earthquakes, it is used as an earthquake precursor because of the possibility to register α particles emitted by increased radon volumetric concentration before strong earthquakes [4–6] within the earthquake preparation zone [7]. One can find many reports on the use of radon as a precursor of strong earthquakes [8–12].

Before considering the effects produced by radon in the atmosphere, we should clarify the ways it is transported to the ground surface [13] and factors influencing its variability [14]. In addition to these factors, we must also consider the dependence of radon activity on weather (precipitation, air pressure, relative humidity, and air temperature), seasonal variability, and space weather effects.

Another important factor is the use of different technologies for radon measurements and the environment in which measurements are taken (soil, water, or surface air layer). The advantages and flaws of alpha and gamma sensors for radon measurements, including gamma spectrometers, should be considered when interpreting radon variations, especially before earthquakes.

To establish the role of radon in our environment, we should also discuss its ionization abilities, including its impact on the Global Electric Circuit [14].

2. Radon Production, Transport, and Gas Migration

Every component of the upper cover of our planet (mantle, crust, and soil) contains some amount of uranium or radium, i.e., sources of radon. For example, every 2.5 km^2 of soil to a depth of 15 cm contains about 1 g of radium, which releases radon into the atmosphere. Only the longest-lived isotope of radon, ^{222}Rn (daughter product of ^{226}Ra, series ^{238}U), whose half-life is 3.8 days, is capable of migrating over any significant distances separately from its parent radionuclides. The concentration of radon in the pores of rocks depends on the uranium (radium) content in them and the emanating ability of the rocks. The release of radon from the solid phase into the pore space (emanation) occurs mainly due to the energy of radioactive recoil. Radon atoms, formed due to alpha decay from radium, experience radioactive recoil and move in the medium. Some of them remain in the solid rock matrix, while some enter pores and cracks and acquire the ability to migrate further. The proportion of radon atoms released into the pore space depends on the distribution of parent radium in the solid phase, the size of solid particles and pores, rock porosity, the content of film and capillary moisture in the pores, and other factors affecting the range of recoil atoms in the medium [15,16].

The transfer of radon in the system of pores and cracks in the lithosphere occurs primarily through two main processes—diffusion and advection. Diffusion is the molecular transfer of radon atoms, it occurs constantly and everywhere if there is a radon concentration gradient, and is most common at the lithosphere–atmosphere interface. The low speed of the diffusion process, combined with the relatively short half-life of radon, significantly limits the distance of its diffusion transfer. Radon can be transported in the lithosphere by diffusion of no more than 10 m before the decay of ^{222}Rn atoms reduces its concentration to a level indistinguishable from the background. At the same time, in areas located outside fault zones, calculations using the classical diffusion model show satisfactory agreement with the measured values of the radon concentration and radon exhalation in the surface soil gas [17,18]. Advection is the volumetric transport of gases under the influence of a wide variety of external forces acting in the lithosphere. The speed and spatial scale of advective transfer of radon is disproportionately greater than diffusion; however, this type of transfer can only be developed in large pores and in fractured fault zones, where the development of intense volumetric gas transfer is possible. The advective gas transport is developed both locally in cracks in the unsaturated zone due to changes in atmospheric pressure, fluctuations in groundwater levels, changes in wind speed and other surface factors, and more globally in fault zones in the presence of significant temperature and pressure gradients. First of all, such conditions are created in areas of modern volcanism in conditions close to the surface of uncooled magma chambers, where volcanic gases are discharged onto the surface [19]. It has also been suggested that changes in stress/strain on fault zones caused by seismic activity may cause crustal fluids to migrate by advection up faults, carrying radon to the surface [20]. In addition, radon anomalies can arise as a result of natural convection of atmospheric air in fault zones in the near-surface part of the lithosphere (above the local erosion base) due to the temperature difference between inside

and outside the mountain range and the surrounding atmosphere (the "stack" effect). This process is not specific to fault zones and occurs in any permeable environment (layers of highly permeable sediments, zones of exogenous fracturing, karst cavities, mine workings), provided there is a temperature gradient between the mountain range and the atmosphere, as well as a difference in heights (outcrops of permeable zones at different elevations above sea level). The rate of convective air transfer at high temperature gradients can reach significant values, which causes the formation of strong radon anomalies even at relatively low contents of uranium and radium in rocks.

Radon is a rare gas with an average concentration in the lithosphere $n \cdot \sim 10^{18}$ mg/kg, and it is not able to form its own gas phase; therefore, radon advection transport occurs as part of a gas mixture contained in pores and cracks (the so-called "geogas"). These are mainly CO_2, CH_4, H_2S, H_2, and other lithospheric gases, which are sometimes called "carrier gases" of radon [21]. It should be remembered that the "carrier" of radon is not any specific gases, but a general gas mixture, the "geogas" that fills the pores and the cracks and moves into them.

The permeability of faults for gas transfer is significantly heterogeneous and depends on many factors, such as the intensity of modern tectonic movements, characteristics of the fracture filler material, water saturation of fractures, and the permeability of surface sediments and soils overlying fault zones [19,22,23]. As a result, radon anomalies above fault zones often represent a chain of individual elongated or isometric degassing spots, apparently confined to the most permeable segments of faults and their intersection points [19]. In such anomalous patches, as a rule, local concentrations of radon in soil gas exceed the levels that would be expected based on the decay of uranium and radium contained in soils [21,24–27]. In most cases, radon concentrations in the soil air above fracture zones slightly exceed the background (up to 2–4 times), which can be satisfactorily explained by increased emanation and more active transfer of gases in fracture zones compared to undisturbed lithosphere blocks. However, there are also strong anomalies, with radon levels exceeding the background by 10–20 times or even several orders of magnitude [28]. According to recently obtained data, such anomalies are associated primarily with the processes of natural convection of atmospheric air in the near-surface part of the lithosphere [29]. A number of large radon anomalies have been recorded over fault zones where uranium ores occur at depths of 100–500 m or more [21,29–32], which suggests the presence in these cases of powerful deep gas flows with which radon is transported from the bowels of the earth over very long distances. Conventional models of advection, much less gas diffusion, cannot explain these facts, since this requires unrealistically high transport rates, especially in water-saturated media. In this regard, the hypothesis of radon bubble transport has been proposed [21,33], according to which radon transfer can occur due to "geogas" bubbles rising upward in water-filled cracks. As they rise, the bubbles "collect" gases dissolved in the water, including radon, transferring them from the liquid phase to the gas phase. Calculations show that theoretically, thanks to this mechanism, rapid transport of radon in the water-saturated lithosphere from the interior to the surface of the Earth over distances of 100–500 m is possible. Bubble transport in some cases actually determines gas exchange in the aquatic environment, for example, in local swamp ecosystems or in the thickness of ocean waters However, there are significantly fewer facts that convincingly indicate the widespread development of this process in fault zones. The correlations between soil radon and the main components of "geogas" (CO_2, CH_4) mentioned by some authors [34] do not in themselves indicate the presence of a bubble transfer mechanism. Experimental observation of bubbles in faults is challenging due to small spatial scales, short time scales, and limited observation conditions [35]. The distance of bubble transfer of ^{222}Rn through a porous material filled with water, obtained in a laboratory experiment, did not exceed 4–5 m, which is at least two orders of magnitude less than the theoretical values [36]. In addition, it is obvious that this mechanism can only be realized under conditions of high gas saturation of water, otherwise the gas will dissolve in water and bubbles simply will not form. All of this limits the possible role of bubble transport in the formation of

radon anomalies in fault zones. A number of authors believe that the above-mentioned strong radon anomalies are not associated with the transfer of radon from deeply buried uranium ores, but are determined by secondary near-surface halos of uranium and radium dispersion [37].

Radon anomalies in fault zones are also characterized by significant temporal variability, including periodic rhythms (seasonal, daily) and non-periodic bursts, as well as sudden changes in the mode and pattern of fluctuations. In most studies, changes in the moisture of the near-surface layer in which measurements are taken are considered as the main cause of seasonal fluctuations in radon, both in fault zones and beyond. In reference [38], various patterns of seasonal fluctuations in radon along the San Andreas fault system (central California, USA) are demonstrated. Four types of anomalous sites were identified in which radon variations were characterized by maximums in winter, maximums in summer, alternation of winter and summer maximums, and sudden non-rhythmic changes in the nature of radon fluctuations. The authors explained seasonal variations in radon by changes in the moisture saturation of surface sediments (depending on the permeability of sediments, infiltrating rainwater reached the depth of the detector installation in summer or winter). The sharp and sudden variations were explained by changes in seismic stresses during the preparation and implementation of earthquakes. In addition, the anomalous seasonal radon fluctuations of radon in fault zones were established, associated with a change in the direction of movement of convective air flows. The change in air movement direction is a result of a seasonal inversion of the temperature gradient between inside and outside the mountain range which can also be characterized by maximums in summer or in winter depending on the elevation above sea level of anomalous sites [29,39]. The seasonal cycle is superimposed by non-periodic fluctuations associated with other reasons, including changes in stress/strain in fault zones caused by seismic and volcanic activity. Thus, a number of studies have recorded a sharp change in the concentration of radon in groundwater and soil gas before strong earthquakes and volcanic eruptions and/or immediately after them [40–43]. The response of the field of radon concentrations to the changes of seismic stresses and deformations cannot yet be considered fully studied; the maximums and minimums of radon concentrations do not always coincide with the time of occurrence of earthquakes. The significant uncertainty is also introduced by the factor of distance from the earthquake source. However, deformations of the environment both during the preparation of an earthquake and during its implementation and propagation of seismic waves undoubtedly create additional pressure gradients and also affect the permeability of the environment, creating additional radon migration paths, which can cause radon emissions into the atmosphere in fault zones during earthquakes, which is confirmed by observational results. The most powerful radon anomalies are observed in areas characterized by both high seismic/volcanic activity and the development of uranium ores or rocks with uranium mineralization.

The problem of radon transport to the surface of ocean and rivers is of special concern. The "geogas" theory resolves one more problem in discussions of the possibility to observe radon over the ocean surface. As a matter of fact, we observe air ionization effects initiated by radon decay both over the land and ocean. The gas migration from the ocean floor resolves this problem, and marine exploration of hydrocarbon proves the presence of carrier gases (at least methane) in the ocean. This problem has not been considered as widely as radon transport over land. Nevertheless, publications have demonstrated the presence of radon both in nearshore waters [44] and in the open ocean [45]. The intensive fluxes of carbon dioxide, i.e., the main carrier of radon from the ocean bottom, can also be considered as radon arising over the ocean surface [46].

3. Multifactor Sources of Radon Variability

Like any natural phenomenon that interacts with the environment, radon is exposed to various factors, the separation of which is a non-trivial task. Simply listing these factors shows the complexity of this task:

1. Various sources of radon (surface layer and deep sources, local anomalies)
2. Ways of bringing radon to the surface (diffusion, transport by geogas and fluids)
3. Place and environment where measurements are taken (underground, in soil, in water, on surfaces indoors, on open surfaces)
4. Atmospheric influences (air humidity, air temperature, atmospheric pressure, air movements—advection and convection)
5. Gravitational deformations (diurnal tides, monthly and seasonal variations)
6. Method of measurement (alpha sensors, gamma sensors, gamma spectrometers)
7. Seismically quiet and seismically active regions.

Looking at the list above, it becomes clear that in order to isolate radon variations associated with the earthquake preparation process, one must filter out all other types of variations listed in the first six points. Moreover, these points are not independent. Each of them is influenced by one or more other factors.

In this section we will try, as a brief overview, to give some idea of the causes of radon variations. All examples will demonstrate that the observed variations are combinations of factors mentioned above.

3.1. Daily Radon Variations

In this paragraph, we will consider two types of radon daily variations: underground and in air. For underground measurements, we will use the results of three very recent publications [47–49]. In publications [47,48], the active air movements in caves and wells play an important role, and the results in general are in good agreement: daily radon variations are controlled by atmospheric parameters, as one can see in Figure 2.
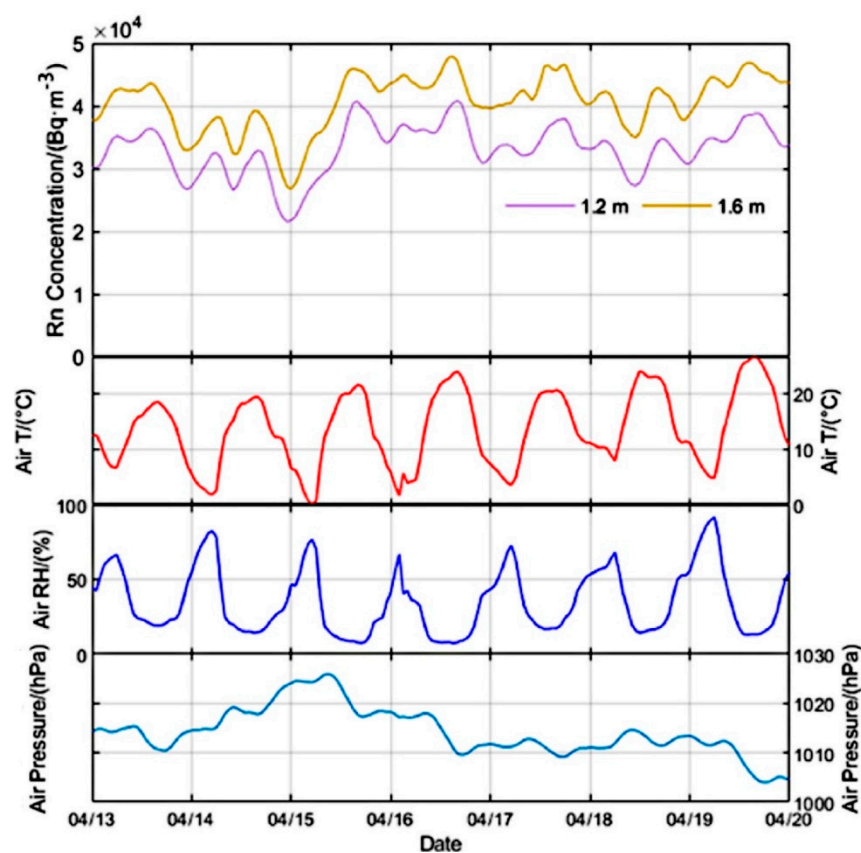

Figure 2. One-week measurement results of radon concentration (3 h moving average) in soil at 1.2 and 1.6 m, air temperature, air relative humidity, and air pressure in typical spring days (13–20 April). The similarity of the results of three publications is due to the fact that caves and wells have the direct contact with the atmosphere [49].

We see the positive correlation with air temperature, and negative correlation with relative humidity and air pressure. The main maximum in radon variations is formed in early afternoon hours, but sometimes we can observe smaller variations in the early morning (3 h) maximum, which will be discussed later.

Seasonal differences are expressed only in the different magnitude of variations, but the correlation characteristics with atmospheric parameters are the same.

Daily variations in radon in air are also controlled by atmospheric behavior, but the main factor is the Global Boundary Layer (GBL) dynamics [50]. This effect was considered in detail in [51] and is presented in Figure 3.
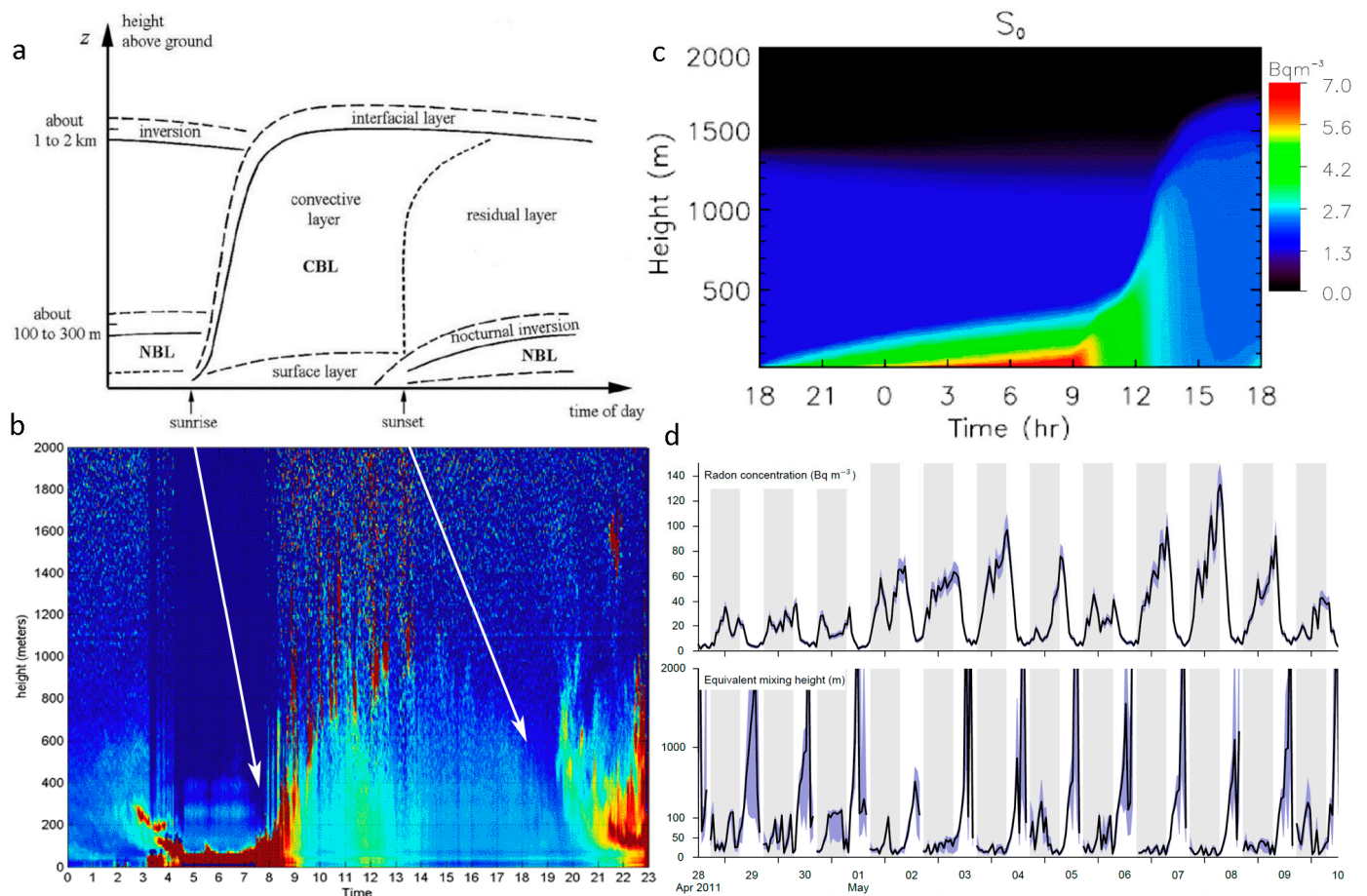
Figure 3. (**a**) Schematic presentation of the GBL daily dynamics [51]. (**b**) Lidar measurements of aerosol concentration in air [52]. (**c**) Modeling of the radon concentration S_0 in local time as a function of GBL dynamics [53]. (**d**) Upper panel: concentration of radon in air; bottom panel: equivalent mixing height during 12 days in April–May 2011 [54].

From Figure 3a, we see that the Nocturnal Boundary Layer (NBL) is located near 100–300 m altitude and vertical motions are suppressed due to the cooling at the surface. We can see this from experimental measurements of daily aerosol dynamics (Figure 3b): the very dense aerosol layer is formed after sunset near 100 m height. Air cooling results in a stable temperature stratification and in the formation of a thin boundary layer isolating the surface from the residual layer above where turbulence decays. The model (Figure 3c) and experimental measurements (Figure 3d) show that the NBL is characterized by very high radon concentrations and significant vertical concentration gradients. During the night, radon is emitted constantly (upper panel of Figure 3d) and, due to the stability of the NBL, it is accumulating close to the surface. After sunrise, due to intensive vertical convection, radon is washed out from the near-ground layer and reaches altitudes up to 2 km (bottom panel of Figure 3d).

Returning to Figure 2, even the underground measurements connected with the atmosphere "feel" the increased radon concentration that is reflected in small maxima mentioned in the legend of Figure 2.

In studies of the air electric conductivity [55] the same night-time radon concentration maximum is marked as a main feature of the radon in air concentration (Figure 4).
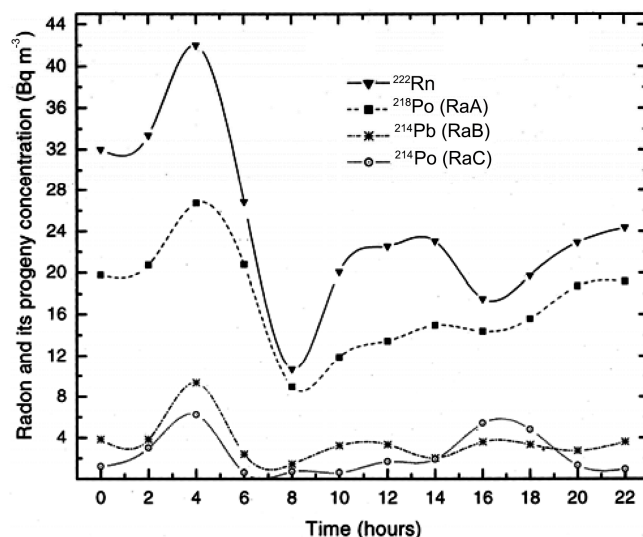

Figure 4. Diurnal variation in radon and its progenies in air [56].

3.2. Seasonal Radon Variations

To come to some conclusion regarding the possible seasonal variations in radon, we used both results of our own measurements and results published in the scientific literature from different regions of the globe: Mt. Beshtau, North Caucasus [40], Northern Altai [56], Black Sea coastal area [57], Israel [58], and Italy [59].

The authors of [39] and [58] conclude that radon concentration follows air temperature and that its maximum is reached during local summer (Figure 5 [39]). In fact, we see the same effect as for daily variation: positive correlation with air temperature and negative correlation with air pressure. Here, two new features could be added. Such variations are characteristic for measurements over the fault (both exhalation rate and radon in air) while average background sites from both sides of the fault do not show changes in exhalation rate (curve b in the top panel). The positive correlation with the temperature difference between the outside air temperature and temperature in the mine where the measurements were taken suggests pumping effects due to the vertical convection initiated by the temperature difference.

The authors of [58] draw similar conclusions indicating that the atmospheric effects are characteristic of the shallow (few meters underground) radon measurements. They discriminate the air temperature and air pressure effects as follows:

- Radon within rock media (as measured by gamma detectors) is driven by the surface temperature gradient to a depth of 100 m, with the same daily cycle and a specific time lag.
- Radon in the measuring air space of open boreholes (as measured by alpha detectors) is driven by pressure. It varies in anti-correlation with the intra-seasonal pressure waves and the semi-daily pressure periodicity.

In [58], another important problem is raised: the difference between the alpha and gamma detector technology in radon monitoring which will be discussed below.

Publications [56,57,59,60] provide the opposite results in seasonal radon variations: winter maximum and summer minimum. Figure 6 shows the radon measurements for the year 2016 in very distant locations: the Black Sea shore (38° E) and Gorny Altai in Siberia

(85.5° E). Variations show surprising similarity: deep minimum in summer season and large sharp intensive variations during winter. Both measurement sites were located in basements isolated from atmospheric variations in air temperature.
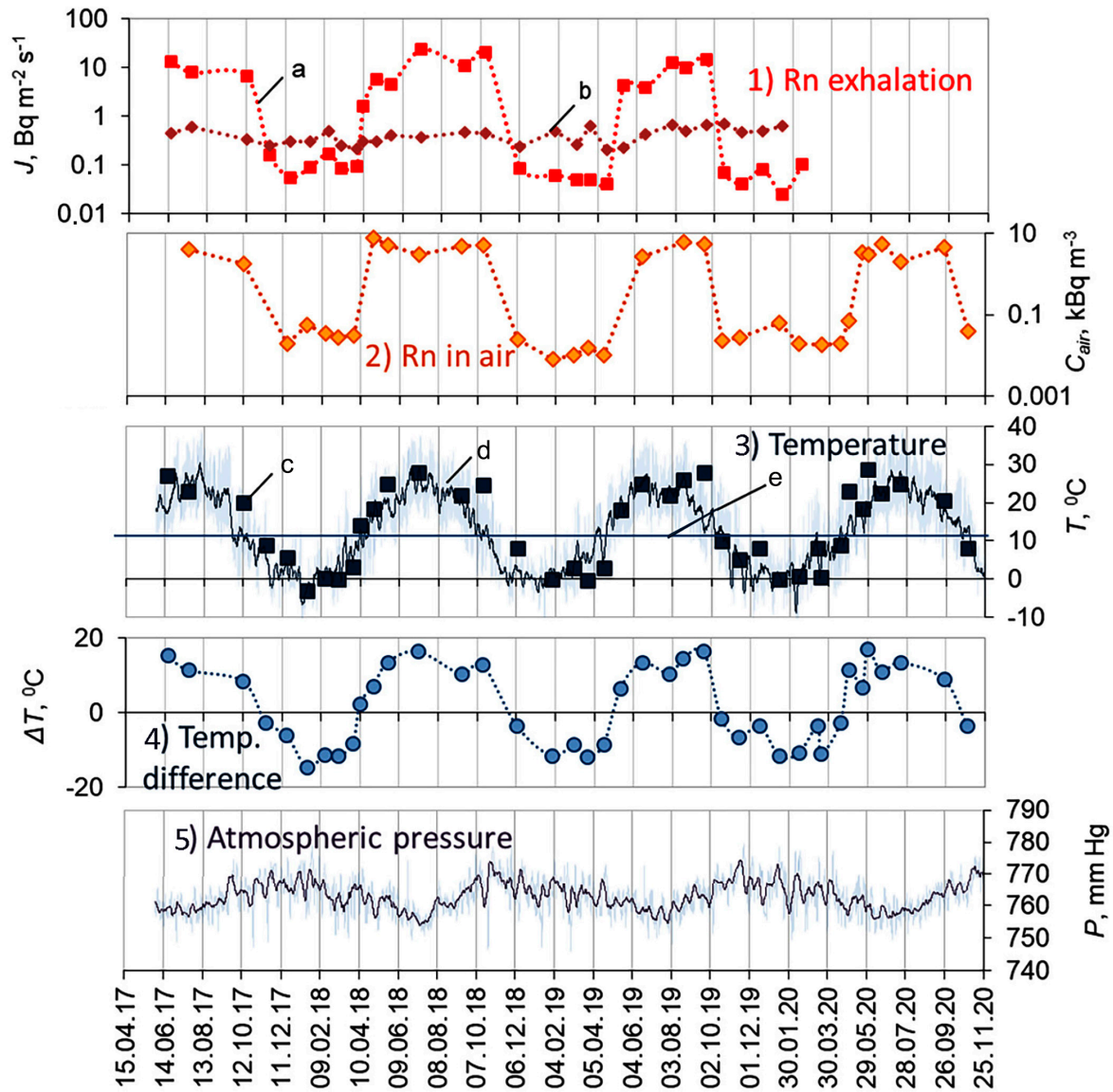

Figure 5. (**1**) Radon exhalation rate from the soil in the fault zone (a)—fault zone, (b)—average for both background sites. (**2**) Variation in radon in air over the fault. (**3**) Air temperature (c)—at the monitoring site, monthly measurements (T_{air}), (d)—data from Mineralnye Vody weather station (MVWS), (e)—average annual temperature inside the mine T_{mine} = 11.5 °C. (**4**) Temperature difference between the outside air temperature and temperature in the mine. (**5**) Atmospheric pressure.

In Italy (Aquila) [59], radon measurements in 2006 were also made in basements, but unlike the first two sites, radon activity was measured by a gamma spectrometer; here again, we see the late summer minimum and the negative correlation with air temperature (Figure 7).
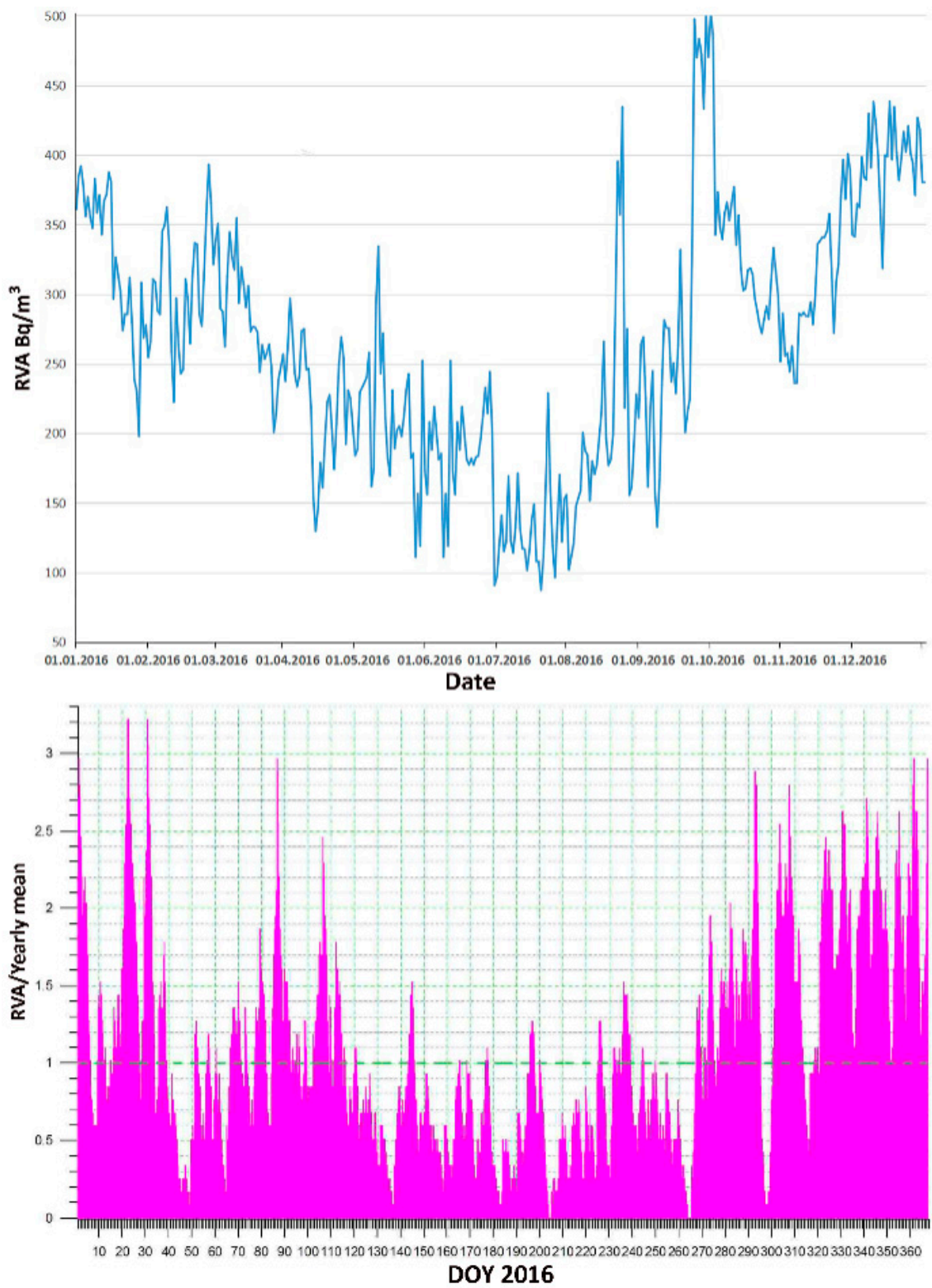
Figure 6. (**Top**) Radon volumetric activity (RVA) at Gorny Altai radon monitoring site. (**Bottom**) Relation of RVA to yearly mean (marked as the bold dashed line) at the Black Sea radon monitoring site (Credit to I. Podymov).
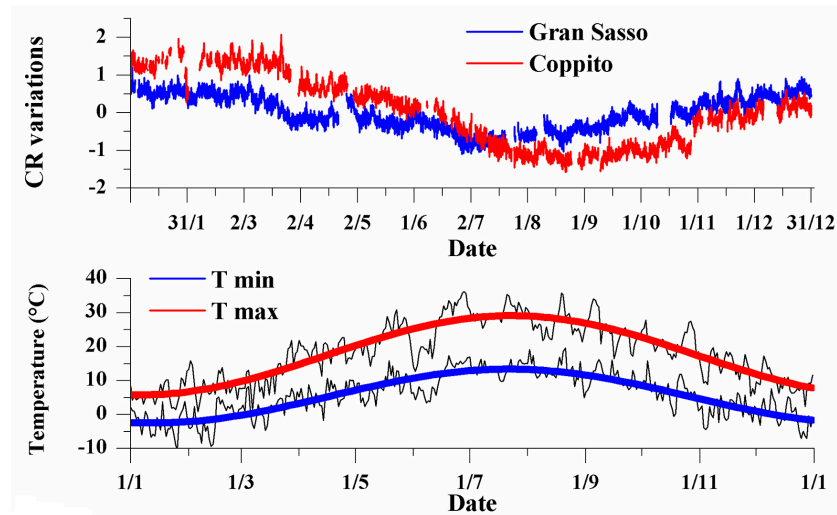
Figure 7. (**Top**) RVA relation to the yearly mean at two sites: Gran Sasso (blue) and Coppito (red) near L'Aquila city. (**Bottom**) Maximum (red) and minimum (blue) air temperature. Black thin lines—the raw measurements. Credit to Giampaolo Giuliani.

Concluding this paragraph, we should state that the seasonal variation in radon activity is controlled by the air temperature both in open space and closed basement sites but with opposite signs of correlation. The explanation for this phenomenon will be the subject of future studies. A control experiment which could be recommended is taking radon measurements at the equator (for example, Singapore or Hawaii), where the temperature is constant through all the year.

3.3. Radon Variations and Solar Activity

It is very difficult find long series of radon measurements throughout the whole solar cycle. One of the most interesting is paper [61], in which the authors calculated the spectra of radon variations within the solar cycle. They found several characteristic periods of radon variations, and naturally, the main peak was near the solar rotation period: 12.39 year^{-1} = 29.3 days. What is the most interesting is that the positive night-time radon variation was established, whose physical mechanism was discussed in [51] and depicted in Figure 2. Actually, the increased radon concentration in the near-ground layer of the atmosphere generates positive deviations in the ionosphere (Figure 8).
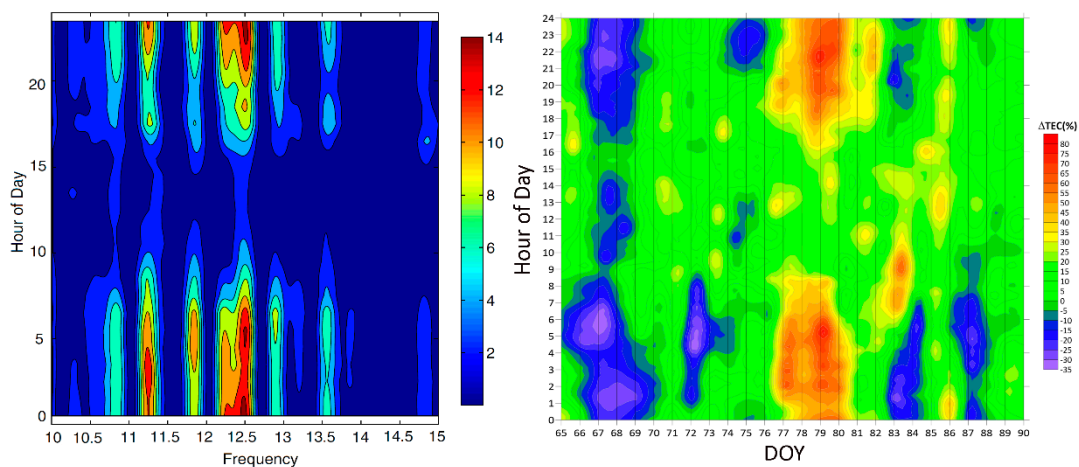

Figure 8. (**Left**) Spectral lines of gamma radon emission versus local time. Modified from [60]. (**Right**) Nocturnal positive ionospheric anomaly off the coast of southern Kamchatka before the M7.5 earthquake of 25 March 2020.

A similar period of 28.5 days was revealed in the long-term radon measurements (2012–2017) at Gorny Altai [56], but it is not a dominating spectrum line in the long-time radon activity registration. The strongest in the observed spectrum is a period of 450 days, which up to now has no reasonable explanation.

The period of continuous observation of the radon activity at Gorny Altai (almost half a solar cycle duration) provides an opportunity to look for a correlation between the RVA and solar activity. The comparison of solar radio flux F10.7 and RVA is presented in Figure 9.
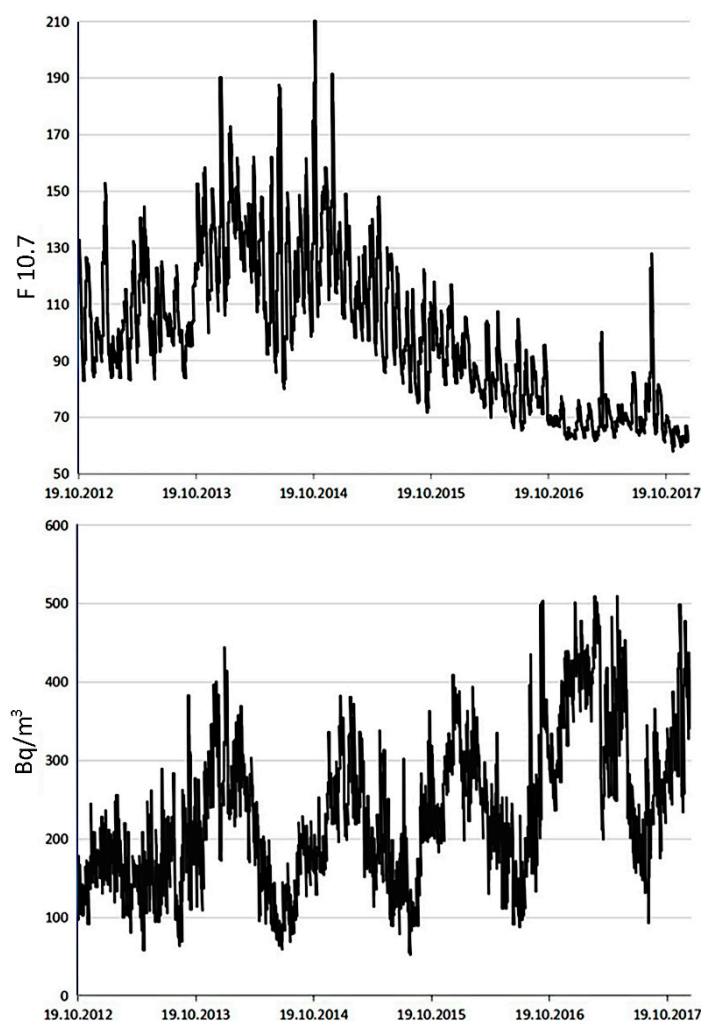

Figure 9. (**Top**) Solar flux F10.7. (**Bottom**) Daily mean RVA.

We can clearly see the counter-directional trends of solar activity and VAR at the end of observational period. Radon activity increases while approaching the minimum of solar activity. The counter-directional trend is only on the surface; in reality, the picture is more complex, as can be seen in Figure 10. The clear negative correlation is revealed in the beginning of the decay phase of the solar cycle in 2014, and in the period approaching the minimum in 2016. Between them, we see the oscillation character of the cross-correlation coefficient, probably modulated by seasonal radon variations.
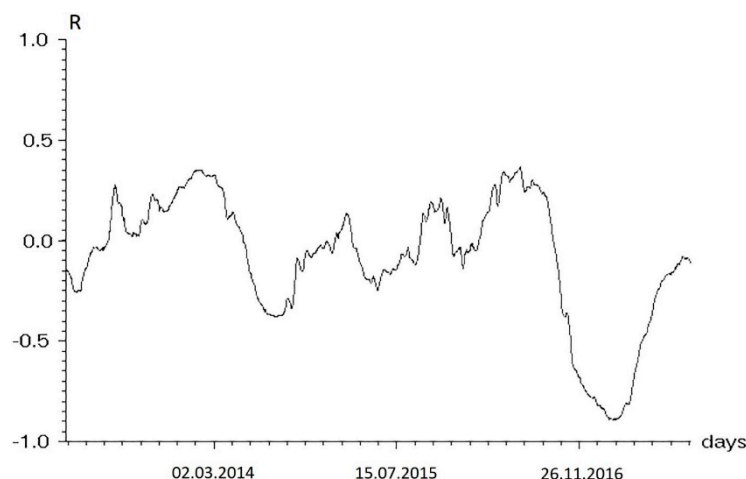
Figure 10. Moving cross-correlation coefficient (R) of the 10.7 index series and the radon volumetric activity series. Sampling frequency is 1 sample/day, sliding time window 200 days, confidence correlation at significance level 0.01, $R_{cr} = 0.1$.

3.4. How to Measure Radon

The history of radon monitoring is very long and starts from ionization chambers, through gas analyzers, to the now widely used alpha sensors and sophisticated gamma spectrometers. These devices currently look like complex stations that also measure air temperature, air pressure, and relative humidity, have smart software and the possibility to be controlled and send information remotely. A separate class of devices are small portable gadgets to measure indoor radon for sanitary purposes.

Another type of instrument category includes passive and active measurements. The first option does not need any operator intervention, and the instrument can operate autonomously and even remotely. The second option involves active operator actions when air should be pumped into the instrument, and this portion of air requires manual chemical analysis.

The problems of radon measurements and discussions about are very old but it seems that paper [62] made the final point in this discussion: the authors demonstrated the clear advantage of gamma sensors, which have a sensitivity 2–4 orders higher than the alpha detectors. Gamma sensors are able to monitor temporal radon variations directly within the geological media without the time delay required for the radon to move and reach equilibrium within the air volume where the alpha detector is located: cave, tunnel, basement, or narrow borehole. The readers can familiarize themselves with this publication, but we want to add something what was not mentioned in it.

First, the most important thing pertains to when we use radon variations as an earthquake precursor. During the years of defamation of physical precursors of earthquakes [63], opponents of forecasts argued that radon was not a harbinger of earthquakes because its anomaly often cannot be registered. However, the problem is not in the absence of radon anomaly before earthquake but in the alpha-particles emitted by the radon-free path in air, which is near 5 cm. This means that the sensor measuring pre-earthquake increase in radon flux should sit directly within this flux, because only a few meters away, it will see nothing. It is quite natural that without knowing the location of an active fault, it is very difficult to "catch" pre-earthquake anomalies. Contrary to alpha emission, the gamma emission is long range and easily penetrating, which means that the gamma sensor will be able to register the radon precursor everywhere within the earthquake preparation zone.

The second important advantage is the possibility to use the gamma spectrometer instead of gamma sensor. Radon itself does not emit gamma quants. Gamma emission is a result of its daughter products. Different radon isotopes (Table 1) produce different daughter products (Figure 1), which, in turn, emit gamma emission producing the rich energy spectrum. We consider that the main isotope to be used as a precursor is ^{222}Rn,

whose daughter products are ^{214}Pb and ^{214}Bi. They emit gamma lines with energies 295 and 352 keV for ^{214}Pb and 609, 1120, and 1764 keV for ^{214}Bi. Thus, if we select only these lines from the total gamma spectrum, we will identify the ^{222}Rn with 100% probability. More details can be found in [59].

One more advantage of a gamma spectrometer placed in an isolated room is that it has no daily amplitude variations correlated with ambient air temperature, contrary to alpha sensor. This is shown in Figure 11, which compares the data series registered by an alpha sensor Rad 7 and a gamma spectrometer PM-4 [59].
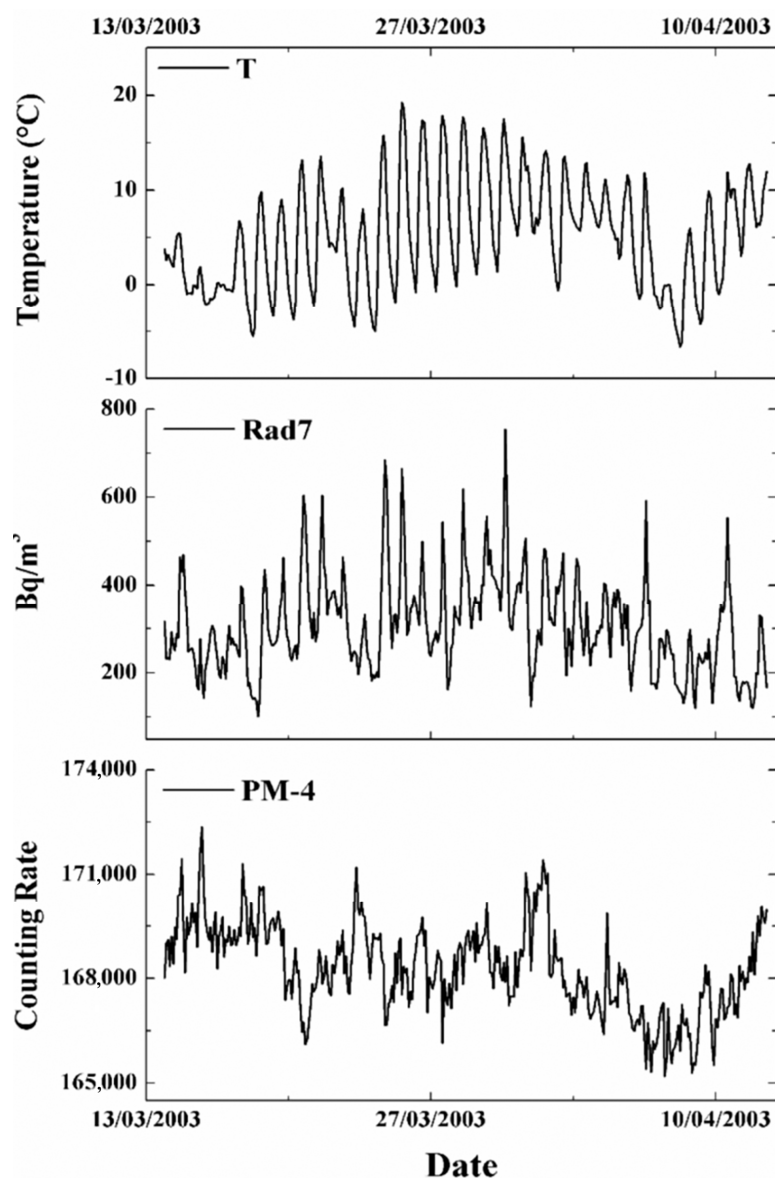

Figure 11. Air temperature, Rad 7, and PM-4 time series [59].

3.5. How to Distinguish Soil and Tectonic Origin Radon

As mentioned above, radon is formed during the decay of radium contained in all layers of the Earth's crust, from the "granite layer" at depths of several kilometers to shallow soils. A natural limitation to the distance over which radon can be transported in the Earth's crust is its relatively short average lifetime, determined by radioactive decay and amounting to 5.5 days. With real speeds of advective transfer of gases in cracks unsaturated with water in the Earth's crust, apparently averaging no more than a few meters per day, and in extreme cases up to 25–35 m/day, the distance over which radon can be transported

to the surface of the Earth with the help of advection averages 20–30 m, in extreme cases perhaps up to 200 m.

However, during radon monitoring, the concentration of radon in soil gas is recorded, as a rule, in near-surface conditions, at a depth of no more than 1 m. In this regard, every time when interpreting the results of radon monitoring, the question arises—What is the nature of the radon that we register with our sensors? Is it formed directly in near-surface soils, in fact, in the area where the measuring device is located, or is all or some part of the recorded radon not of local origin, but arrives through advective transport to the surface along faults from greater depths? In the case of some other gases, for example, He, CO_2, or CH_4, the answer to the question of the depth and genesis of the gas can to a certain extent be given by the isotope ratios of helium and carbon. However, in the case of radon, such isotopic tracers are absent. Radon atoms formed directly at the surface of the Earth and in the deep parts of the Earth's crust do not differ from each other.

At the same time, it is possible to distinguish between radon of soil and tectonic (deeper) origin based on the analysis of data from simultaneous monitoring of radon concentration in soil gas at a depth of 0.5 to 1 m and the radon exhalation rate from the soil surface.

As we have established during experiments on radon monitoring, in the case when radon is formed directly in the near-surface soil layer, an inverse correlation is observed between the concentration of radon in soil gas and the rate of radon exhalation from the soil surface: with an increase in radon exhalation from the surface, its concentration in the soil gas decreases (top panel of Figure 12). This is logical, because the more radon that flows out of the soil, the less of it remains in the soil air. This type of correlation is typical for areas located outside fault zones, characterized, as a rule, by a relatively thick layer of soils overlying bedrock, where diffusive transfer of radon predominates [17,18,64]. Most often, fluctuations in soil radon under such conditions are caused by changes in soil permeability, which is associated, in turn, with fluctuations in air temperature and soil moisture. A decrease in permeability leads to an increase in radon exhalation and an increase in the concentration of radon in soil gas, and vice versa, a decrease in soil permeability causes an increase in exhalation and a decrease in the concentration of radon in the soil.

In the case when radon is transferred to the near-surface zone along cracks from deeper horizons, including radon of tectonic origin, the nature of the correlation between the concentration of radon in soil gas and the rate of radon exhalation from the surface is of the opposite nature. There is a direct correlation between these parameters (lower panel of Figure 12). This is due to the fact that in this case, radon enters the near-surface layer, where measurements are taken, with an advective gas flow from a certain depth, which leads to a synchronous change in both the radon concentration at a depth of 0.5–1.0 m and the exhalation speed of radon from the Earth's surface. This type of correlation is observed in highly permeable zones of tectonic faults [18,29]. Under such conditions, high-amplitude synchronous fluctuations in the concentration of radon in soil gas and exhalation of radon from the surface are observed, which, as a rule, are closely correlated with air temperature.

Additional information about the sources of radon is provided by measurements of the content of [226]Ra, the parent of radon, in the near-surface soil layer where the sensors are located. Thus, the totality of information about fluctuations in radon concentration in soil gas, the rate of radon exhalation from the soil surface, and the radium content in these soils makes it possible to attempt to separate radon of soil and tectonic origin during gas-dynamic monitoring. The first of such studies show their high promise [18,39].
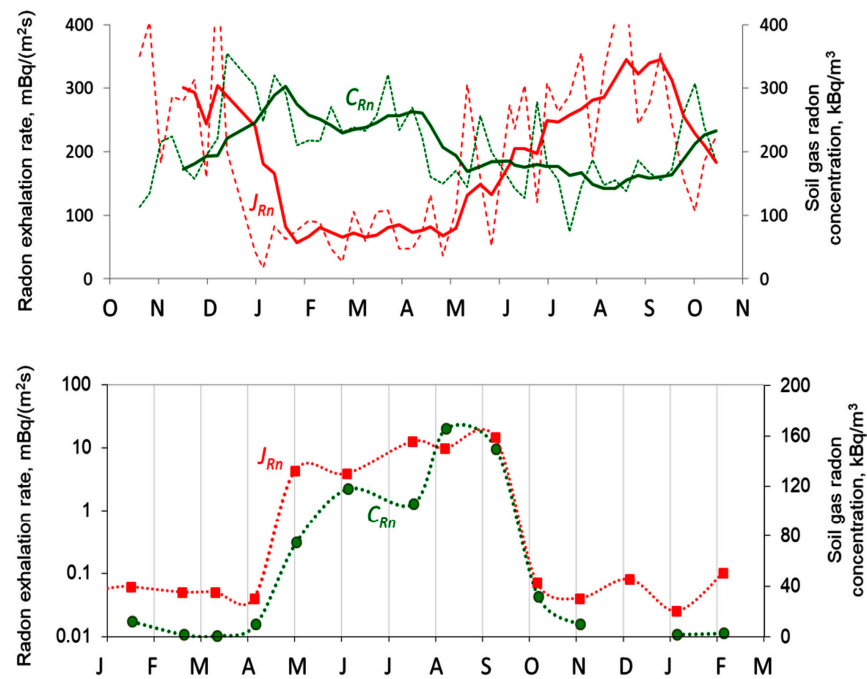
Figure 12. Fluctuations in the rate of radon exhalation (J_{Rn}) and radon concentration in soil gas (C_{Rn}) in the area with radon of soil origin outside the fault zones (**upper** panel) and in the area with convective transfer of radon in the fault zone (**lower** panel). Dashed lines in the upper panel are the raw measurements.

4. Radon as Diagnostic Means and an Earthquake Precursor

From the discussion above we see that radon reacts to variations in atmospheric parameters. This means that by solving the inverse problem, we can try to determine atmospheric parameters based on measurements of radon variations [65]. In this publication Robertson demonstrates the different atmospheric borders and air movements where radon can be used as a tracer (Figure 13).
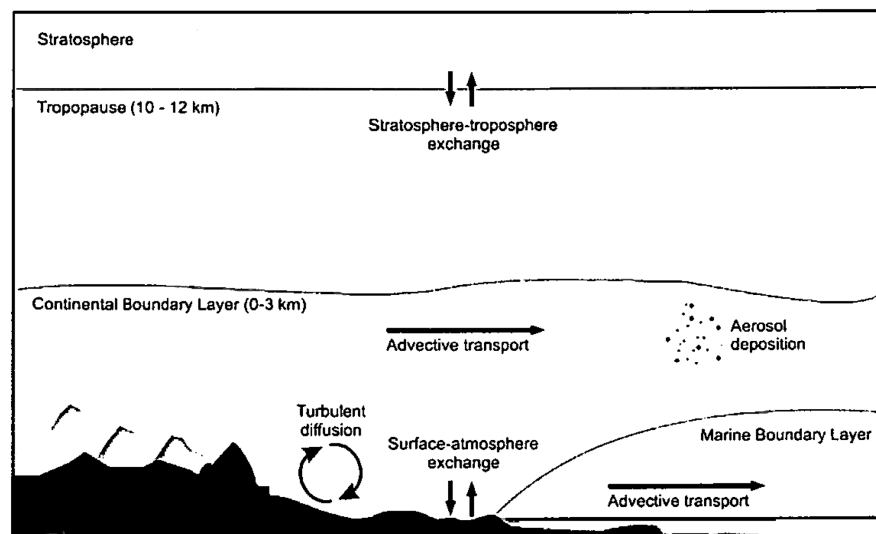

Figure 13. Schematic illustration of the various atmospheric transport processes for which ^{222}Rn and its radioactive decay products are used as tracers.

As it was mentioned above, radon emanation is now used as a tracer of the upper border of the Global Boundary Layer of the atmosphere.

Gamma emission within the energy band of [214]Bi 484–800 keV, the daughter of [222]Rn was used to monitor the spatial distribution of crustal activity in Japan during 8 years [66]. The gamma scintillation counter RE-100 was installed close to the earth surface while moving by car or Shinkansen bullet train on the route from Kyoto to Tokyo. This monitoring showed a long-term increasing trend in radon concentration in Inagawa Town, Hyogo Prefecture, from around the end of 2001 with a rate of 16/count/min/year. An increase in the level of radon emanation by 22% was also revealed in particular regions near Kyoto.

4.1. Radon Activity as a Measure of Tectonic Stress

When filtering radon variations caused by meteorological factors and air movements the question arises: are the residual variations in radon concentration (including variations before earthquakes), both increasing and decreasing, connected only with the transport of radon through the new ways of migration, or can the rock deformation itself change the radon emanation effectiveness? Paper [67] provides an answer to this question. It presents the results of laboratory experiments on the effects of radon emanation changes after mechanical and thermal damage of various granite representatives of the upper crust. In comparison with other experiments using one-dimensional loading, the authors of [67] used three-dimensional deformation when the samples were placed under natural conditions (controlled confinement and pore pressure), and then they were flushed with pore gas. Their results show that radon emanation increases up to $170 \pm 22\%$ at the last moments before the sample rupture. At the same time, heating of the sample to 850 °C shows that thermal fracturing irreversibly decreases emanation by 59–97% due to the amorphization of biotites hosting radon sources. Thus, we can conclude that the temporal radon variations before earthquakes are the result of two effects: new ways of gas (and fluid) migration and changes in radon emanation from solid bodies under increasing stress and temperature.

Is there any possibility to check the stress-radon release relation not only in laboratory experiments but in natural conditions besides earthquakes? The closest to the seismic cycle conditions and well-controlled experiments were produced with transient deformation near reservoir lakes [68]. It is reported that the electric potential, radon emanation, and deformation measurements recorded since 1995 in the French Alps vary in the vicinity of two artificial lakes, which have strong seasonal variations in water level of more than 50 m. In both emptying and filling of water reservoirs during transition periods, increased radon emanation was observed.

In [69], the authors tested the dependence of the radon emanation intensity on the tectonic fault parameters. Emanation survey results for Central Mongolia and the Baikal region show that faults and their key parameters, such as size rank, internal structure peculiarities, dynamic formation conditions, and seismic activity, have a significant effect on radon activity. Additional analysis of the radon survey data from other regions confirms the discovered regularities. Dependence of radon emanation intensity on fault parameters is shown in Figure 14.

The correction of the atmospheric chemical potential (ACP) parameter (discussed below) was derived from studies of radon ionization effects on the lower atmosphere [70], and it was demonstrated that it can be used as a radon activity proxy [71]. It follows, with a high level of correlation, the tectonic shear traction [72], which was checked by mutual global monitoring. Figure 15 demonstrates the variations in ACP (blue and green) and share traction around the time of the Fukushima earthquake on 16 March 2022.
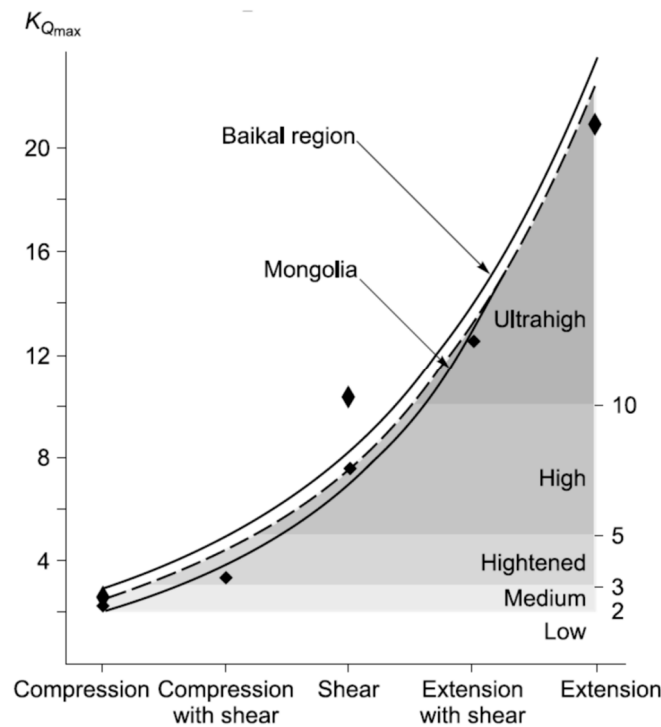
Figure 14. Diagram illustrating the effect of dynamic formation conditions of faults in Mongolia and the Baikal region on maximum radon activity values ($K_{Q\,max}$) identified for each group of tectonic faults. Gray scale represents radon activity levels of faults according to the accepted classification [69].
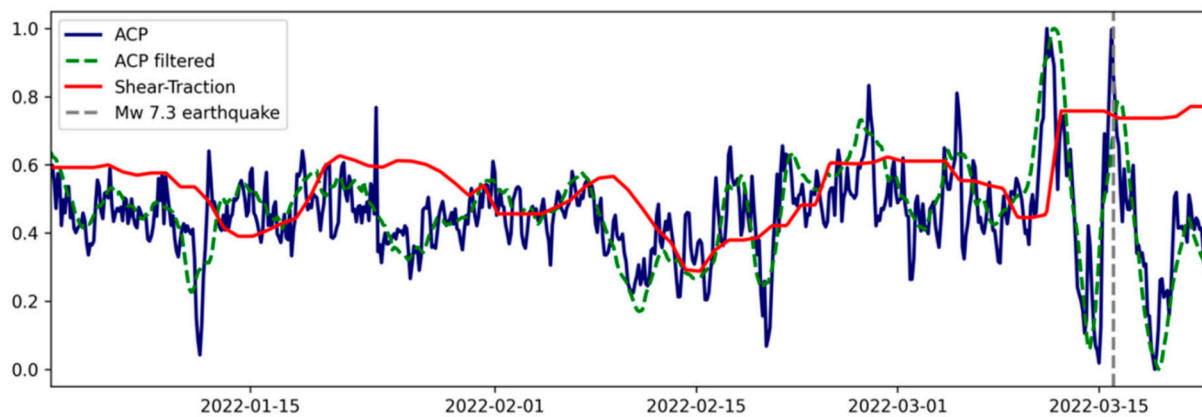

Figure 15. Average of near- and intermediate-field of ACP (unfiltered—blue; filtered—green) and shear-traction field (red) in the epicentral area of the 16 March 2022 Fukushima earthquake, Japan (time shown with grey vertical dashed line). The ACP follows the temporal evolution of the shear-traction field before the earthquake, while the spike in ACP occurs at the same time and shear traction increases.

We obtained enough proof that radon reacts to deformation in the Earth's crust, including laboratory experiments [67], natural monitoring of tectonic fault activity [69], artificial stress initiation due to large water reservoirs filling and emptying [68], and global monitoring of shear stress with the radon proxy [72]. The paper length limitations prevent us from providing more examples, but even from the examples provided, it is clear that radon-stress effects can be used in practical applications including short-term earthquake forecasts.

Organization of earthquake forecasts using radon variations is not the subject of the present paper. We will only demonstrate what forecast parameters can be estimated using the radon variations.

4.2. Radon as an Earthquake Precursor

For correct forecasts, we need to determine three main parameters: time, location, and magnitude. We have many examples of pre-earthquake radon anomalies. Some recent examples include [73–75]. But for real forecasts, these values should be determined with sufficient precision. What does this mean? For example, the leading time of the pre-earthquake anomaly should be sufficiently stable. Otherwise, the time spread makes parameter values insignificant. Of course, in different areas of seismic activity, the leading time value can be different, but for the given place it should be stable. Figure 16 shows results of radon in air monitoring in Azov and Black Seas area.
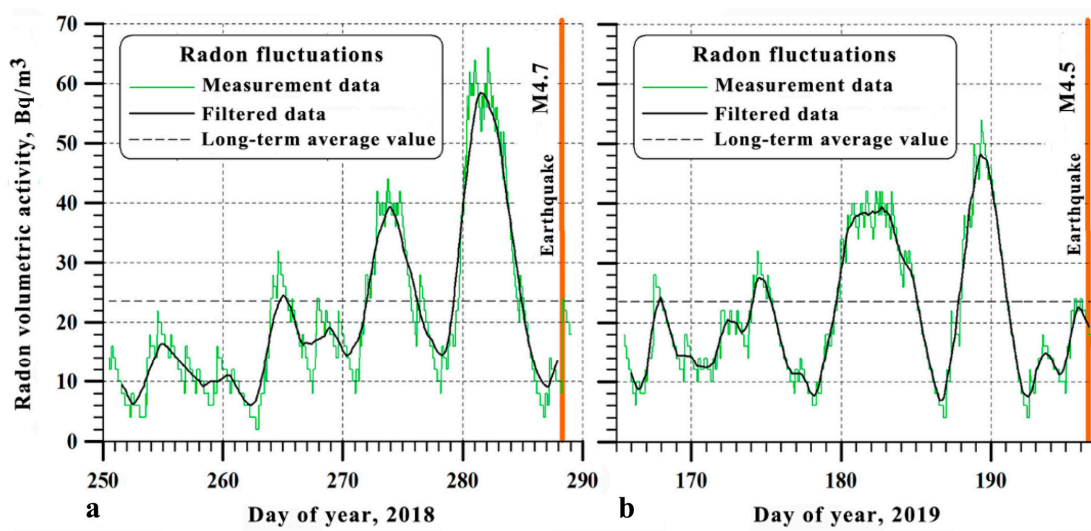

Figure 16. Charts of radon volumetric activity fluctuations in the near-surface atmosphere: (**a**) 38 days before the earthquake in the Sea of Azov; (**b**) 32 days before the earthquake in the Black Sea [75].

One can clearly see that the main maximum of radon pre-earthquake variation for both cases have a leading time of nearly 6 days.

It is difficult to find the epicenter position from single-sensor radon measurements. In this case we can use the radon proxy ACP, which is calculated from assimilative atmospheric models; with its help, we can obtain its spatial distribution within the zone of earthquake preparation. Figure 17 shows the ACP spatial distribution map one day before the M6.3 earthquake 34 km from Herat, Afghanistan.

The same approach of ACP distribution is used for earthquake magnitude estimation assuming that the radius of the ACP anomaly is on the order of the Dobrovolsky earthquake preparation zone radius [7] determined as:

$$R(km) = 10^{0.43M} \tag{1}$$

where M is the earthquake magnitude

This estimate is based on the fact that spatial radon distribution determined statistically from many publications on radon monitoring in seismically active regions follows the Dobrovolsky law of magnitude–size relationship [7], as demonstrated in Figure 18.
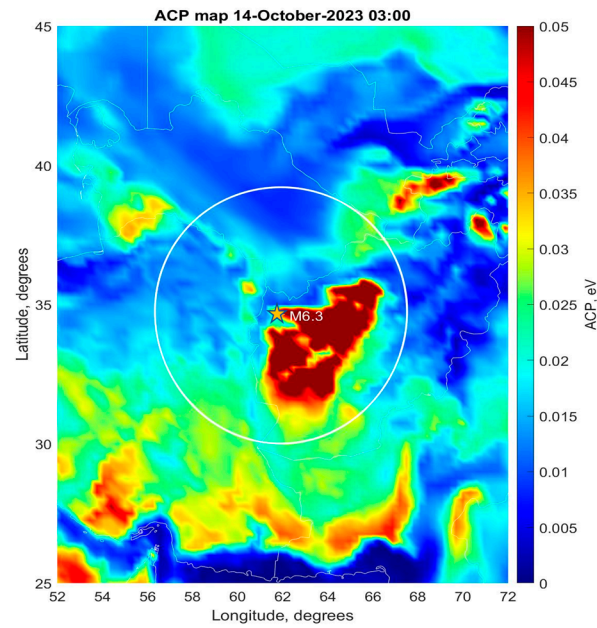
Figure 17. Spatial distribution of ACP one day before the M6.3 earthquake in Afghanistan on 15 October 2023. Epicenter position is shown by the orange star, and the white circle indicates the earthquake preparation zone for M6.3.
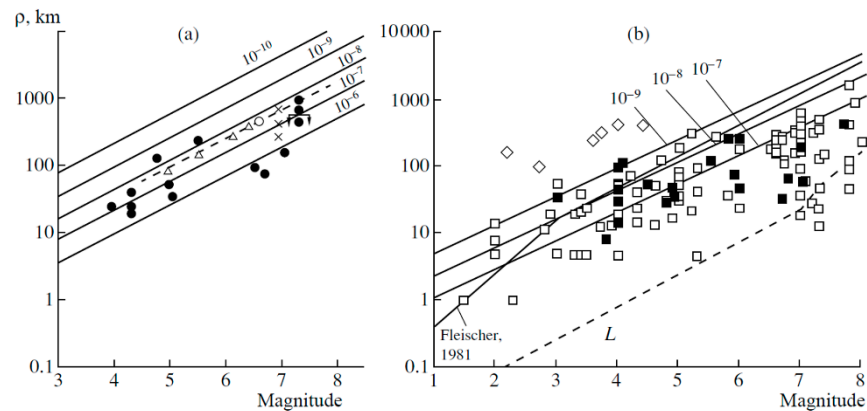

Figure 18. (**a**) Distance from the precursor to the epicenter as a function of earthquake magnitude. Geochemical precursors are denoted by filled circles; the resistance from different sources, by dashes and crosses; telluric currents, by triangles; radon, by arrows; and light effects, by open circles. Modified from [7]. (**b**) Distance from the precursor to the epicenter as a function of the earthquake magnitude for geochemical data. Modified from [5]. Opened and filled squares denote measurements of radon and other gaseous anomalies, respectively. Continuous thin lines show the relation between the deformation radius and magnitude for deformations of 10^{-7} to 10^{-9} in accordance with the empirical Equation (1). The thick line represents the empirical dependence derived in [76] as a result of calibrating the maximal distance between the measured anomaly and epicenter for a given magnitude on the basis of the shear dislocation law for earthquakes. The dashed line shows the typical size of the rupture zone of an active fault as a function of magnitude in accordance with the empirical equation of Aki and Richards [77].

Another indicator for earthquake magnitude estimation can be the amplitude and duration of the radon anomaly, but this question needs more statistical studies.

5. Radon as a Component of the Global Electric Circuit

The Global Electric Circuit (GEC) exists due to two major processes: creating the potential difference of nearly 250 kV between the ionosphere at altitude ~80 km and

ground surface created by the global thunderstorm activity [78] and the existence of air conductivity which provides the fair weather vertical current from the ionosphere to the Earth's surface due to air ionization by external sources (galactic cosmic rays, solar proton events, magnetospheric electrons and protons, and solar electromagnetic emission) and an internal source, i.e., natural ground radioactivity, where radon plays the major role [14,79].

To estimate the radon contribution in air ionization is not a simple task because the real global distribution of radon is very rough. Nevertheless, such an attempt was made in [80]. The author used the chemistry–climate model SOCOLv3 [81] considering ionization by solar energetic particles during an extreme solar proton event (SPE), galactic cosmic rays (GCR), and terrestrial radon (^{222}Rn).

Contribution of radon in air ionization is calculated as:

$$IR = ((CRn\text{-}222 \times 10^{-3})/5.69 \times 10^{15}) \times \rho \qquad (2)$$

where CRn-222 is the ratio of the mass of ^{222}Rn to the mass of dry air; 5.69×10^{15} Bq is the conversion factor between mBq/(m^2·s) and g/(m^2·s) (1 g ^{222}Rn in the calculation corresponds to 5.69×10^{15} Bq); and ρ is air density (kg/m^3).

The global distribution of the ionization rate at an altitude 1000 hPa (near ground surface) according to the model distribution of radon emanation is presented in Figure 19.
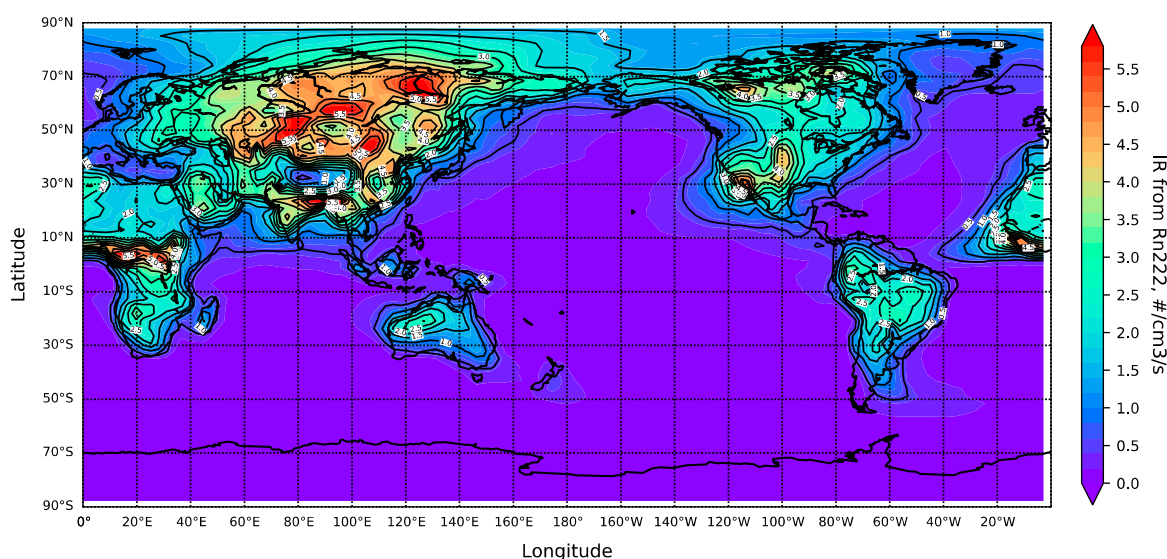

Figure 19. Global distribution of atmospheric ionization rates at an altitude of 1000 hPa caused by ^{222}Rn emissions averaged over January 2005, calculated using the SOCOLv3 chemical–climate model. Reprinted from [80], with permission from A.V. Karagodin.

It should be mentioned that at the regional level, models exist based on real measurements. The radon activity map for Russia is presented in the Figure 20 [82].

Figure 19 shows that the ionization rates from radon do not exceed values of the order of 6 ion pairs/cm^3/s, and the highest ionization rates caused by radon emissions are observed in individual foci in the territories of Eurasia, part of Africa, and the west coast of North America. The average values of radon ionization rates obtained in the SOCOLv3 model were compared with other results obtained previously in other models [83,84]. The comparison showed good consistency of results in terms of the order of magnitude and distribution of radon on the surface. Since the ground surface in ocean areas is covered by water, there is a very low level of ionization caused by radon over the surface of the oceans. Only in coastal areas close to the continents is there an increased level of ionization from ^{222}Rn, due to radon transport by rivers [44].
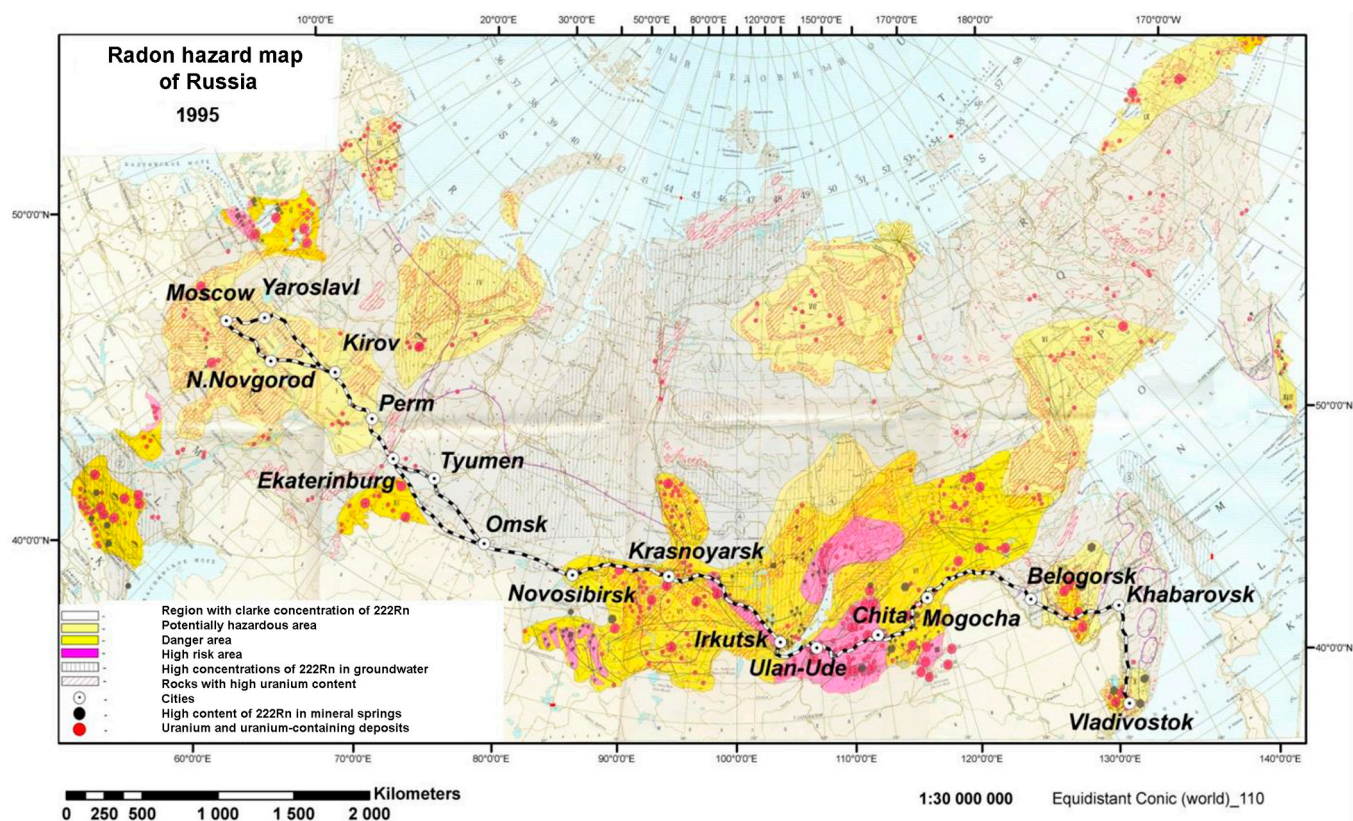
Figure 20. Radon hazard map of Russia for 1995. Modified from [82].

According to [85], we calculate the air conductivity as:

$$\sigma = n \times e \times (\mu^- + \mu^+), \tag{3}$$

where: σ—specific conductivity (Sm/m); n—total number of ion pairs from all included sources (cm^3); e—elementary charge (C); $\mu^- + \mu^+$—mobility of positive and negative ions (in our work, we assume an equal number of negative and positive ions). Three separate numerical experiments were carried out in which conductivity was calculated for each of the three ionization sources in order to estimate the contribution of each of the considered natural ionization sources to the overall conductivity of the atmosphere. The calculation results are presented in Figure 21. To calculate ionization rates from fluxes of galactic cosmic rays (GCR), solar cosmic rays (SCR), and solar proton events (SPE), the CRAC model CRII was used [85,86]. Figure 21 shows calculations of atmospheric conductivity caused by ^{222}Rn, GCR, and SPS through the SOCOLv3 model. In Figure 21, two SPEs are considered, one on 17 January 2005 and another SPE of the ground level enhancement (GLE) type on 20 January 2005. SCR flows are considered on undisturbed/quiet days from 1 January to 15 January 2005.

From Figure 21, it is clear that above 50 hPa, the predominant contribution to the ionization rate is made by ionization from the event of 20 January 2005. Ionization from radon is the main contributor to conductivity only in the layer of the atmosphere that is closest to the Earth's surface, somewhere below 850–900 hPa. In general, ionization has an exponential dependence and grows from the Earth's surface, where it has an average global value of the order of 10^{-13}, and to the upper boundary of the model atmosphere, where the conductivity value grows to values on the order of 10^{-7}, which corresponds to observations and previously obtained numerical results [84]. To compare the specific conductivity during the disturbed period (for 17 and 20 January 2005), the specific conductivity was also calculated for ionization from SCR during the quiet period. The time period from 1–15 January 2005 was chosen as the quiet period. It can be seen from the figure that the

conductivity during the quiet period differs from the conductivity during the disturbed period by approximately two to three orders of magnitude, depending on the height. This modeling study took into account all of the main natural sources of atmospheric ionization and took into account the contribution to atmospheric conductivity from a solar event compared to quiet conditions.
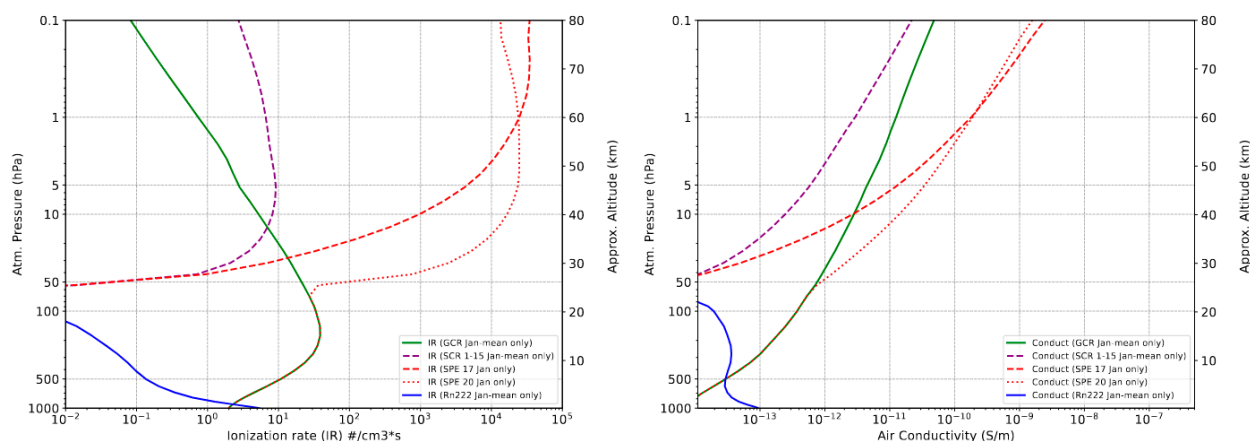

Figure 21. (**Left**) Global average ionization rates from various sources. Red lines: Ionization rates from the SPE on 17 January (dashed line) and 20 January (dotted line) 2005; purple dotted line: SCR ionization rate on undisturbed/quiet days (1–15 January 2005); green curve: ionization rate from GCR (averaged for January 2005); blue curve: ionization rate from ^{222}Rn (averaged over January 2005). (**Right**) Global average contribution of various ionization sources to the total atmospheric conductivity. Red lines: conductivity caused by ionization from the ATP on 17 January (dashed line) and 20 January (dotted line) 2005; purple dotted line: conductivity caused by ionization from SCR on undisturbed/quiet days (1–15 January 2005); green curve: conductivity calculated using ionization from GCR (averaged for January 2005); blue curve: conductivity calculated using ionization from ^{222}Rn (averaged over January 2005). Reprinted from [80], with permission from A.V. Karagodin.

Looking at the results of modeling, a reader may not notice anything unusual; however, something that was never acknowledged before is that air ionization by radon produces an essential impact on the GEC parameters. In Figure 22, the computed latitudinal distribution of the vertical fair-weather current is shown at a longitude near 1° W.

The difference between calculated fair-weather current density taking into account only GCR ionization and fair-weather current density taking into account radon and the GCR effect is about 0.2–0.6 pA/m^2 and appears in the ^{222}Rn active regions, see [14]. It is an essential contribution that should create a local anomaly of the ionosphere potential.

We made model calculations using a commonly accepted radon concentration on the ground surface of nearly 3 Bq/m^3, but in the Figure 16, we see values close to 60 Bq/m^3 which were measured at 2 m altitude above the ground surface. It is more than an order of magnitude larger than the radon concentration used in calculations. Some time ago, we provided radon measurements in a closed box to prevent wind effects at 3 levels: −70 cm, 0 cm, and 100 cm in relation to ground surface in two different regions of Mexico [87]. The results are presented in Table 2. Altitude −70 cm is the level where the original ground radon concentration was measured. From these values at the ground surface, we see concentrations reaching 288 Bq/m^3, which is two orders of magnitude larger than accepted in the calculations. At the altitude of 100 cm, radon concentrations are similar to those presented in Figure 16 from the Azov and Black Sea shore areas.
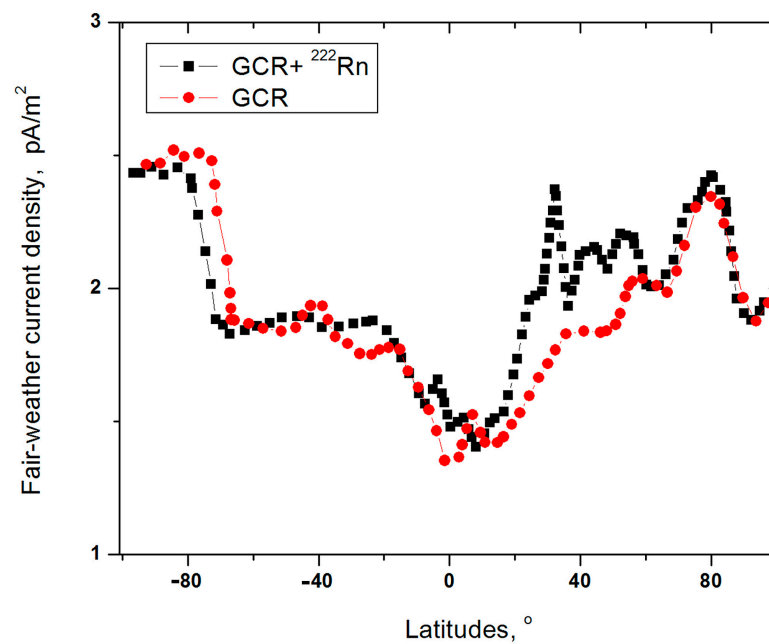
Figure 22. Fair-weather current density calculated for June 2005. Red line: fair-weather current taking into account only GCR ionization effect; black line: fair-weather current taking into account radon and the GCR effect. Figure is modified from [14].

Table 2. Radon concentration values in Bq·m^{-3}: average (Av) and relative standard deviations (RSD) in percentage (Av $\pm$ RSD (%)), maximum (Max), and minimum (Min)values obtained at 70 cm below the surface (-70 cm), at the surface (0 cm), and at 100 cm above the surface, in air [87].

Location	-70 cm			0 cm			100 cm		
	Max	**Min**	**Av $\pm$ RSD**	**Max**	**Min**	**Av $\pm$ RSD**	**Max**	**Min**	**Av $\pm$ RSD**
Cuernavaca (Bq m^{-3})	4813	873	2249 $\pm$ 71	288	86	179 $\pm$ 48	37	20	29 $\pm$ 6
% original soil radon	100	100	100	6	10	8	0.8	2.3	1.3
Las Cruces (Bq m^{-3})	3197	500	1574 $\pm$ 64	159	59	106 $\pm$ 33	18	17	18 $\pm$ 4
% original soil radon	100	100	100	5	12	6.7	0.5	3.4	1.1

The future direction of our work in radon ionization ability will concentrate on areas of increased radon concentration to calculate local anomalies of the ionospheric potential.

6. Conclusions

In this research, we tried to create a comprehensive picture of radon variations under action of different factors. We demonstrated that meteorological effects have important contributions to radon variations. It was revealed that effects also depend on the sensor location, e.g., closed spaces or directly connected with the atmosphere (even in caves). The convection direction depending on the temperature difference between outside and inside of a room where the sensor is located my change the sign of dependence on air temperature and pressure. The main results of this consideration are as follows:

1. Meteorological effects depend not only on the pure variations in meteorological parameters but also on the methodology and location of radon measurements (pumping effect) and differences between outside and inside (where the sensor is installed) temperatures

2. Daily radon variability (night-time maximum) is determined by daily dynamics of the Global Boundary Layer
3. Two types of seasonal variation in radon (summer maximum or minimum) need further clarification. The summer maximum is likely a result of measurement site location. The summer minimum should be checked by long-time measurements at the geodetic equator where the air temperature does not change throughout the year

Tectonic activity also has different methods of action on radon concentration. Stress works at a microlevel and can change the level of radon emanation, increasing it by 177% (in laboratory experiments), and increases in the crust temperature lead to decreases in radon emanation. In addition, large-scale deformations can create new ways of gas transport within the crust, leading to changing the levels of radon exhalation at the ground surface. Thus, radon exhalation intensity should depend on the earthquake source mechanism: extension, compression, or shear. During the preparation period, we can observe the increase or decrease in radon flux intensity, or even no changes.

It was demonstrated that there are two types of radon origin:

1. The surface radon contained in radium grains of the soil
2. Tectonic radon coming from deeper layers of the crust. The problem with many publications is that dependence of surface radon on meteorological parameters is applied to tectonic radon, creating a 'mish-mash' in data interpretation
3. One of the new and important results is the way of discriminating between surface and tectonic radon. It is simple but effective: for surface radon, the radon concentration and exhalation are in counterphase, while for the tectonic radon, they are in phase.

The solar activity effects on radon activity were practically not studied in the literature; here we made two contributions:

1. We supplemented the description in [60] of the oscillation of radon intensity within the solar cycle with a maximum period of 12.5 years, which is modulated by radon changes in local time. The maximum of radon activity is observed during night-time hours, coinciding with variations in the Total Electron Content provided by radon activity.
2. The study of long-term observations of radon activity in Gorny Altai implies the possible anticorrelation of solar and radon activity within the solar cycle. Nevertheless, more long-term observation analyses are necessary to make a more definite conclusion.

Advantage of gamma spectrometry for ^{222}Rn monitoring and discriminating from other radon isotopes and daughter products was demonstrated.

The role of radon in environmental monitoring applications was highlighted. It is used as a tracer for determining the upper boundary of the Global Boundary Layer and as an earthquake precursor.

One of the more significant results of this publication is a demonstration of the importance of radon contribution to the vertical current–ionospheric potential of the global electric circuit. It opens the way to further improvement of the Lithosphere–Atmosphere–Ionosphere Coupling (LAIC) model where the GEC plays an important role in the atmosphere–ionosphere coupling mechanism.

All results mentioned above are not considered final and will be improved and developed in future work.

Author Contributions: Methodology, P.M. and A.S.; Validation, I.M. and P.M.; Formal analysis, T.P. and A.K.; Investigation, S.P., I.M., P.M., T.P., A.S. and A.K.; Data curation, T.P., A.S. and A.K.; Writing—original draft, S.P.; Supervision, S.P. All authors have read and agreed to the published version of the manuscript.

References

1. Dorn, F.E. Über die von radioaktiven Substanzen ausgesandte Emanation. *Ges. Zur Halle* **1900**, *22*, 155.
2. Rutherford, E.; Owens, R.B. Thorium and uranium radiation. *Trans. R. Soc. Can.* **1899**, *2*, 9–12.
3. Debierne, A.-L. Sur la radioactivite induite provoquee par les sels d'actinium. *Comptes Rendus Hebd. Des Séances De L'académie Des Sci.* **1903**, *136*, 446.
4. Scholz, C.H.; Sykes, L.R.; Aggarwal, Y.P. Earthquake prediction: A physical basis. *Science* **1973**, *181*, 803–809. [CrossRef] [PubMed]
5. Toutain, J.-P.; Baubron, J.-C. Gas geochemistry and seismotectonics: A review. *Tectonophysics* **1998**, *304*, 1–27. [CrossRef]
6. Steinitz, G.; Begin, Z.B.; Gazit-Yaari, N. Statistically significant relation between radon flux and weak earthquakes in the Dead Sea rift valley. *Geology* **2003**, *31*, 505–508. [CrossRef]
7. Dobrovolsky, I.P.; Zubkov, S.I.; Myachkin, V.I. Estimation of the size of earthquake preparation zones. *Pure Appl. Geophys.* **1979**, *117*, 1025–1044. [CrossRef]
8. Allegri, L.; Bella, F.; Della Monica, G.; Ermini, A.; Impora, S.; Sgrigna, V.; Biagi, P.F. Radon and tilt anomalies detected before the Irpinia (South Italy) earthquake of 23 November 1980 at great distance from the epicenter. *Geophys. Res. Lett.* **1983**, *10*, 269–272. [CrossRef]
9. Igarashi, G.; Saeki, S.; Takahata, N.; Sumikawa, K.; Tasaka, S.; Sasaki, Y.; Takahashi, M.; Sano, Y. Ground-Water Radon Anomaly Before the Kobe Earthquake in Japan. *Science* **1995**, *269*, 60–61. [CrossRef]
10. King, C.-Y. Gas geochemistry applied to earthquake prediction. An overview. *J. Geophys. Res.* **1996**, *91*, 12269–12281. [CrossRef]
11. Ghosh, D.; Deb, A.; Sengupta, R. Anomalous radon emission as precursor of earthquake. *J. Appl. Geophys.* **2009**, *69*, 67–81. [CrossRef]
12. Yasuoka, Y.; Nagahama, H.; Ishikawa, T. Anomalous Radon Concentration Prior to an Earthquake. A case Study on the 1995 Kobe Earthquake, Japan. In *Collected Papers*; LAMBERT Academic Publishing: Saarbrücken, Germany, 2010; 138p.
13. Khilyuk, L.F.; Chilingar, G.V.; Robertson, J.O., Jr.; Endres, B. Gas migration. In *Events Preceding Earthquakes*; Gulf Publishing Company: Houston, TX, USA, 2000; 342p.
14. Golubenko, K.; Rozanov, E.; Mironova, I.; Karagodin, A.; Usoskin, I. Natural Sources of Ionization and Their Impact on Atmospheric Electricity. *Geophys. Res. Lett.* **2020**, *47*, e2020GL088619. [CrossRef]
15. Miklyaev, P.S.; Petrova, T.B. Studies of radon emanation from clays. *Water Resour.* **2011**, *38*, 868–875. [CrossRef]
16. Baskaran, M. Mechanisms of Radon Emanation and Long-Term Radon Flux Studies. In *Radon: A Tracer for Geological, Geophysical and Geochemical Studies*; Springer: Berlin/Heidelberg, Germany, 2016; pp. 37–62.
17. Marenny, A.M.; Tsapalov, A.A.; Miklyaev, P.S.; Petrova, T.B. *Regularities of Formation of the Radon Field in the Geological Environment*; "Pero" Publishing House: Moscow, Russia, 2016; 394p.
18. Gavriliev, S.; Petrova, T.; Miklyaev, P.; Karfidova, E. Predicting radon flux density from soil surface using machine learning and GIS data. *Sci. Total Environ.* **2023**, *903*, 166348. [CrossRef]
19. Ciotoli, G.; Lombardi, S.; Annunziatellis, A. Geostatistical analysis of soil gas data in a high seismic intermontane basin: Fucino Plain, Central Italy. *J. Geophys. Res.* **2007**, *112*, B05407. [CrossRef]
20. King, C.-Y.; King, B.-S.; Evans, W.; Zhang, W. Spatial radon anomalies on active faults in California. *Appl. Geochem.* **1996**, *11*, 497–510. [CrossRef]
21. Etiope, G.; Martinelli, G. Migration of carrier and trace gases in the geosphere: An overview. *Phys. Earth Planet. Inter.* **2002**, *129*, 185–204. [CrossRef]

22. Annunziatellis, A.; Beaubien, S.; Bigi, S.; Ciotoli, G.; Coltella, M.; Lombardi, S. Gas migration along fault systems and through the vadose zone in the Latera caldera (central Italy): Implications for CO_2 geological storage. *Int. J. Greenh. Gas Control* **2008**, *2*, 353–372. [CrossRef]

23. Richon, P.; Klinger, Y.; Tapponnier, P.; Li, C.-X.; Van Der Woerd, J.; Perrier, F. Measuring radon flux across active faults: Relevance of excavating and possibility of satellite discharges. *Radiat. Meas.* **2010**, *45*, 211–218. [CrossRef]

24. Ball, T.K.; Cameron, D.G.; Colman, T.B.; Roberts, P.D. Behavior of radon in the geological environment: A review. *Q. J. Eng. Geol. Hydrogeol.* **1991**, *2*, 169–182. [CrossRef]

25. Walia, V.; Lin, S.J.; Fu, C.C.; Yang, T.F.; Hong, W.L.; Wena, K.L.; Chen, C.H. Soil–gas monitoring: A tool for fault delineation studies along hsinhua fault (Taiwan), southern Taiwan. *Appl. Geochem.* **2010**, *25*, 602–607. [CrossRef]

26. Moreno, V.; Bach, J.; Font, L.; Baixeras, C.; Zarroca, M.; Linares, R.; Roqué, C. Soil radon dynamics in the Amer fault zone: An example of very high seasonal variations. *J. Environ. Radioact.* **2016**, *151*, 293–303. [CrossRef]

27. Chen, Z.; Li, Y.; Liu, Z.; Wang, J.; Zhou, X.; Du, J. Radon emission from soil gases in the active fault zones in the Capital of China and its environmental effects. *Sci. Rep.* **2018**, *8*, 16772. [CrossRef]

28. Kobeissi, M.A.; Gomez, F.; Tabet, C. Measurement of Anomalous Radon Gas Emanation Across the Yammouneh Fault in Southern Lebanon: A Possible Approach to Earthquake Prediction. *Int. J. Disaster Risk Sci.* **2015**, *6*, 250–266. [CrossRef]

29. Miklyaev, P.; Petrova, T.; Marennyy, A.; Shchitov, D.; Sidyakin, P.; Murzabekov, M.; Lopatin, M. High seasonal variations of the radon exhalation from soil surface in the fault zones (Baikal and North Caucasus regions). *J. Environ. Radioact.* **2020**, *219*, 106271. [CrossRef] [PubMed]

30. Gingrich, J.E. Results from a new uranium exploration method. *Trans. AIME* **1975**, *258*, 61–64.

31. Gingrich, J.E.; Fisher, J.C. *Uranium Exploration Using the Track-Etch Method*; Symposium on Exploration of Uranium Ore Deposits; International Atomic Energy Agency (IAEA): Vienna, Austria, 1976; SM-208/19; pp. 213–225.

32. Fleischer, R.L.; Mogro-Campero, A. Mapping of integrated radon emanation for detection of long-distance migration of gases within the Earth: Techniques and principles. *J. Geophys. Res.* **1978**, *83*, 3539–3549. [CrossRef]

33. Chen, X.; Liu, Y.; Jiang, Y.; Feng, S. Radon transport carried by geogas: Prediction model. *Environ. Sci. Pollut. Res.* **2023**, *30*, 86656–86675. [CrossRef]

34. Berberich, G.M.; Berberich, M.B.; Ellison, A.M.; Wöhler, C. Degassing Rhythms and Fluctuations of Geogenic Gases in A Red Wood-Ant Nest and in Soil in The Neuwied Basin (East Eifel Volcanic Field, Germany). *Insects* **2018**, *9*, 135. [CrossRef]

35. Cao, H.; Jia, X.; Li, Y.; Amador, C.; Ding, Y. CFD-DNS simulation of irregular-shaped particle dissolution. *Particuology* **2020**, *50*, 144–155. [CrossRef]

36. Vàrhegyi, A.; Hakl, J.; Monnin, M.; Morin, J.; Seidel, J. Experimental study of radon transport in water as test for a transportation microbubble model. *J. Appl. Geophys.* **1992**, *29*, 37–46. [CrossRef]

37. Novikov, G.F. *Radiometric Scouting*; Nedra: Leningrad, Russia, 1989; 407p.

38. King, C.Y.; Minissale, A. Soil variability of soil-gas radon concentration of cenrtal California. *Radiat. Meas.* **1994**, *23*, 683–692. [CrossRef]

39. Miklyaev, P.S.; Petrova, T.B.; Shchitov, D.V.; Sidyakin, P.A.; Murzabekov, M.A.; Tsebro, D.N.; Marennyy, A.M.; Nefedov, N.A.; Gavriliev, S.G. Radon transport in permeable geological environments. *Sci. Total Environ.* **2022**, *852*, 158382. [CrossRef]

40. Firstov, P.P.; Makarov, E.O.; Glukhova, I.P. Parameter Variations in the Subsoil Radon Field at the Paratunka Station of the Petropavlovsk-Kamchatsky Geodynamic Test Site in 2011–2016. *Seism. Instrum.* **2018**, *54*, 121–133. [CrossRef]

41. Utkin, V.I.; Yurkov, A.K. Radon as a "Deterministic" indicator of natural and industrial geodynamic processes. *Dokl. Earth Sci.* **2009**, *427*, 833–836. [CrossRef]

42. Kats, V.E.; Shitov, A.V.; Drachev, S.S. On the mechanisms of changes in the chemical composition and temperature of groundwater in the Gorno-Altaisk region. *Geoecology Eng. Geol. Hydrogeol. Geocryol.* **2010**, *3*, 207–212.

43. Ciotoli, G.; Bigi, S.; Tartarello, C.; Sacco, P.; Lombardi, S.; Ascione, A.; Mazzoli, S. Soil gas distribution in the main coseismic surface rupture zone of the 1980, M_s = 6.9, Irpinia earthquake (southern Italy). *J. Geophys. Res. Solid Earth* **2014**, *119*, 2440–2461. [CrossRef]

44. Jacob, N.; Suresh Babu, D.S.; Shivanna, K. Radon as an indicator of submarine groundwater discharge in coastal regions. *Curr. Sci.* **2009**, *97*, 1313–1320.

45. Kawabata, H.; Narita, H.; Harada, K.; Tsunogai, S.; Kusakabe, M. Air-Sea Gas Transfer Velocity in Stormy Winter Estimated from Radon Deficiency. *J. Oceanogr.* **2003**, *59*, 651–661. [CrossRef]

46. Marty, B.; Tolstikhin, I.N. CO_2 fluxes from mid-ocean ridges, arcs and plumes. *Chem. Geol.* **1998**, *145*, 233–248. [CrossRef]

47. Levintal, E.; Dragila, M.I.; Zafrir, H.; Weisbrod, N. The role of atmospheric conditions in CO_2 and radon emissions from an abandoned water well. *Sci. Total Environ.* **2020**, *722*, 137857. [CrossRef]

48. Benkovitz, A.; Zafrir, H.; Reuveni, Y. The dynamics of Rn-222 cyclic flow within the shallow geological subsurface media as a daily temporal variated source for exhalation into the air. *Sci. Total Environ.* **2024**, *912*, 169244. [CrossRef] [PubMed]

49. Mao, Y.; Zhang, L.; Wang, H.; Guo, Q. The temporal variation of radon concentration at different depths of soil: A case study in Beijing. *J. Environ. Radioact.* **2023**, *264*, 107200. [CrossRef] [PubMed]

50. Cushman-Roisin, B. Atmospheric boundary layer. In *Environment Fluid Dynamics*; John Wiley & Sons, Inc.: Hoboken, NJ, USA, 2014; pp. 165–186.

51. Pulinets, S.A.; Davidenko, D.V. The Nocturnal Positive Ionospheric Anomaly of Electron Density as a Short-Term Earthquake Precursor and the Possible Physical Mechanism of Its Formation. *Geomagn. Aeron.* **2018**, *58*, 559–570. [CrossRef]

52. Eresmaa, N.; Härkönen, J.; Joffre, S.M.; Schultz, D.M.; Karppinen, A.; Kukkonen, J. A Three-Step Method for Estimating the Mixing Height Using Ceilometer Data from the Helsinki Testbed. *J. Appl. Meteorol. Clim.* **2012**, *51*, 2172–2187. [CrossRef]

53. Vinuesa, J.-F.; Basu, S.; Galmarini, S. The diurnal evolution of 222Rn and its progeny in the atmospheric boundary layer during the Wangara experiment. *Atmos. Chem. Phys.* **2007**, *7*, 5003–5019. [CrossRef]

54. Griffiths, A.D.; Parkes, S.D.; Chambers, S.D.; McCabe, M.F.; Williams, A.G. Improved mixing height monitoring through a combination of lidar and radon measurements. *Atmos. Meas. Tech.* **2013**, *6*, 207–218. [CrossRef]

55. Chandrashekara, M.S; Sannappa, J.; Paramesh, L. Electrical conductivity of air related to ion pair production rate from radon and its progeny concentrations in dwellings of Mysore city. *Indian J. Pure Appl. Phys.* **2005**, *43*, 679–683.

56. Shitov, A.V. *The Influence of Regional and Global Geophysical Characteristics on the Volumetric Activity of Radon in Gorno-Altaisk (Russia); Radon: Detection, Exposure and Control*; Nova Science Publishers: Hauppauge, NY, USA, 2020; pp. 19–30.

57. Podymov, I.; Podymova, T. Seasonal variability of radon volumetric activity in the surface layer of the atmosphere of the Black Sea coast. In Proceedings of the MSOI-2017, Jeunesse Arena, Brazil, 28 April–21 May 2017. [CrossRef]

58. Zafrir, H.; Barbosa, S.M.; Malik, U. Differentiation between the effect of temperature and pressure on radon within the subsurface geological media. *Radiat. Meas.* **2013**, *49*, 39–56. [CrossRef]

59. Giuliani, G.G.; Attanasio, A.; Fioravanti, G. Gamma Detectors for Continuous Monitoring of Radon. *J. Int. Environ. Appl. Sci.* **2013**, *8*, 541–550.

60. Belete, G.D.; Shiferaw, A.M. A Review of Studies on the Seasonal Variation of Indoor Radon-222 Concentration. *Oncol. Rev.* **2022**, *16*, 10570. [CrossRef] [PubMed]

61. Sturrock, P.; Steinitz, G.; Fischbach, E.; Javorsek, D.; Jenkins, J. Analysis of gamma radiation from a radon source: Indications of a solar influence. *Astropart. Phys.* **2012**, *36*, 18–25. [CrossRef]

62. Zafrir, H.; Haquin, G.; Malik, U.; Barbosa, S.; Piatibratova, O.; Steinitz, G. Gamma versus alpha sensors for Rn-222 long-term monitoring in geological environments. *Radiat. Meas.* **2011**, *46*, 611–620. [CrossRef]

63. Geller, R.J.; Jackson, D.D.; Kagan, Y.Y.; Mulargia, F. Earthquakes Cannot Be Predicted. *Science* **1997**, *275*, 1616–1618. [CrossRef]

64. Neznal, M.; Neznal, M. Measurement of Radon Exhalation Rate from the Ground Surface: Can the Parameter Be Used for a Determination of Radon Potential of Soils? *Radon Investigations in the Czech Republic IX.* 2002, pp. 16–25. Available online: https://www.radon-vos.cz/pdf/radon_inv_9-2002.pdf (accessed on 20 January 2024).

65. Robertson, L.B. Radon Emissions to the Atmosphere and Their Use as an Atmospheric Tracer. Ph.D. Thesis, College of Science and Engineering, Institute of Atmospheric and Environmental Science, School of GeoSciences, The University of Edinburg, Edinburgh, UK, 2004; 221p.

66. Tsukuda, T. Radon-gas Monitoring by Gamma-ray Measurements on the Ground for Detecting Crustal Activity Changes. *Bull. Earthq. Res. Inst. Univ. Tokyo* **2008**, *83*, 227–241.

67. Nicolas, A.; Girault, F.; Schubnel, A.; Pili, É.; Passelègue, F.; Fortin, J.; Deldicque, D. Radon emanation from brittle fracturing in granites under upper crustal conditions. *Geophys. Res. Lett.* **2014**, *41*, 5436–5443. [CrossRef]

68. Trique, M.; Richon, P.; Perrier, F.; Avouac, J.P.; Sabroux, J.C. Radon emanation and electric potential variations associated with transient deformation near reservoir lakes. *Nature* **1999**, *399*, 137–141. [CrossRef]

69. Seminsky, K.; Bobrov, A.; Demberel, S. Radon and Tectonic Activities of Crustal Faults: The Case of Central Mongolia. *Russ. Geol. Geophys.* **2019**, *60*, 204–214. [CrossRef]

70. Pulinets, S.A.; Ouzounov, D.P.; Karelin, A.V.; Davidenko, D.V. Physical bases of the generation of short-term earthquake precursors: A complex model of ionization-induced geophysical processes in the lithosphere-atmosphere-ionosphere-magnetosphere system. *Geomagn. Aeron.* **2015**, *55*, 521–538. [CrossRef]

71. Pulinets, S.; Ouzounov, D.; Karelin, A.; Boyarchuk, K. *Earthquake Precursors in the Atmosphere and Ionosphere*; New Concepts; Springer Nature: Berlin, Germany, 2022; 312p. Available online: https://link.springer.com/book/10.1007/978-94-024-2172-9 (accessed on 20 January 2024).

72. Pulinets, S.; Vičič, B.; Budnikov, P.; Potočnik, M.; Dolenec, M.; Žalohar, J. Correlation between Shear-Traction field and Atmospheric Chemical Potential as a tool for earthquake forecasting. In Proceedings of the 3rd European Conference on Earthquake Engineering and Seismology, Bucharest, Romania, 4–9 September 2022; pp. 3623–3627.

73. Hwa Oh, Y.; Kim, G. A radon-thoron isotope pair as a reliable earthquake precursor. *Sci. Rep.* **2015**, *5*, 13084. [CrossRef]

74. Gregorič, A.; Zmazek, B.; Džeroski, S.; Torkar, D.; Vaupotič, J. Ch. 9 Radon as an Earthquake Precursor—Methods for Detecting Anomalies. In *Earthquake Research and Analysis—Statistical Studies, Observations and Planning*; D'Amico, S., Ed.; InTech: London, UK, 2012; pp. 179–196. [CrossRef]

75. Podymov, I.S.; Podymova, T.M.; Esin, N.V. Infrared Radiation of Thermal Anomalies and Radon Fluctuation Anomalies Preceding Two Earthquakes in the Sea of Azov and the Black Sea. *Ecol. Saf. Coast. Shelf Zones Sea* **2020**, *2*, 41–52. (In Russian) [CrossRef]

76. Fleischer, R.I. Dislocation model for radon response to distance earthquakes. *Geophys. Res. Lett.* **1981**, *8*, 477–480. [CrossRef]

77. Aki, K.; Richards, P.G. *Quantitative Seismology*; Theory and Methods; Freeman: New York, NY, USA, 1980; 948p.

78. Ilin, N.V.; Slyunyaev, N.N.; Mareev, E.A. Toward a Realistic Representation of Global Electric Circuit Generators in Models of Atmospheric Dynamics. *J. Geophys. Res. Atmos.* **2020**, *125*, e2019JD032130. [CrossRef]

79. Eisenbud, M.; Gesell, T. *Environmental Radioactivity: From Natural, Industrial, and Military Sources*, 4th ed.; San Diego Academic Press: San Diego, CA, USA, 1997; 688p.
80. Karagodin, A.V. Impact of Space Factors on Processes in the Global Electric Circuit. Ph.D. Thesis, Saint Petersburg State University, Saint Petersburg, Russia, 2022; 109p. Available online: https://disser.spbu.ru/files/2022/disser_karagodin.pdf (accessed on 20 January 2024).
81. Stenke, A.; Schraner, M.; Rozanov, E.; Egorova, T.; Luo, B.; Peter, T. The SOCOL version 3.0 chemistry-climate model: Description, evaluation, and implications from an advanced transport algorithm. *Geosci. Model Dev. Discuss.* **2012**, *5*, 3419–3467. [CrossRef]
82. Maksimovsky, V.A.; Reshetov, V.V.; Kharlamov, M.G. *Radon Hazard Map of Russia*; Scale 1:10,000,000; Smyslova, A.A.-M.-S., Ed.; St. Petersburg State Mining Institute: St. Petersburg, FL, USA, 1995; 1p.
83. Tinsley, B.A.; Zhou, L. Initial results of a global circuit model with variable stratospheric and tropospheric aerosols. *J. Geophys. Res.* **2006**, *111*, D16205. [CrossRef]
84. Lucas, G.M.; Baumgaertner, A.J.G.; Thayer, J.P. A global electric circuit model within a community climate model. *J. Geophys. Res. Atmos.* **2015**, *120*, 12054–12066. [CrossRef]
85. Usoskin, I.G.; Kovaltsov, G.A. Cosmic ray induced ionization in the atmosphere: Full modeling and practical applications. *J. Geophys. Res.* **2006**, *111*, D21206. [CrossRef]
86. Usoskin, I.G.; Kovaltsov, G.A.; Mironova, I.A. Cosmic ray induced ionization model CRAC:CRII: An extension to the upper atmosphere. *J. Geophys. Res. Atmos.* **2010**, *115*, D10302. [CrossRef]
87. Segovia, N.; Pulinets, S.; Leyva, A.; Mena, M.; Monnin, M.; Camacho, M.; Ponciano, M.; Fernandez, V. Ground radon exhalation, an electrostatic contribution for upper atmospheric layers processes. *Radiat. Meas.* **2005**, *40*, 670–672. [CrossRef]